

 Open access • Journal Article • DOI:10.1063/1.470096

## Trajectory simulations of collisional energy transfer in highly excited benzene and hexafluorobenzene — [Source link](#)





[Thomas Lenzer](#), [Klaus Luther](#), [Jürgen Troe](#), [Robert G. Gilbert](#) ...+1 more authors

**Published on:** 08 Jul 1995 - [Journal of Chemical Physics](#) (American Institute of Physics)

**Topics:** [Hexafluorobenzene](#), [Rotational energy](#), [Excited state](#), [Xenon](#) and [Ground state](#)

Related papers:

- [Energy transfer in highly excited large polyatomic molecules](#)
- [Quasiclassical trajectory study of collisional energy transfer in toluene systems. I. Argon bath gas: Energy dependence and isotope effects](#)
- [Collisional energy transfer in the low-pressure-limit unimolecular dissociation of HO<sub>2</sub>](#)
- [Collisional energy transfer probabilities of highly excited molecules from kinetically controlled selective ionization \(KCSI\). II. The collisional relaxation of toluene: P\(E',E\) and moments of energy transfer for energies up to 50 000 cm<sup>-1</sup>](#)
- [Vibrational energy transfer](#)

Share this paper:    

View more about this paper here: <https://typeset.io/papers/trajectory-simulations-of-collisional-energy-transfer-in-371ufg23l3>

## Trajectory simulations of collisional energy transfer in highly excited benzene and hexafluorobenzene

Thomas Lenzer, Klaus Luther, Jürgen Troe, Robert G. Gilbert, and Kieran F. Lim

Citation: *The Journal of Chemical Physics* **103**, 626 (1995); doi: 10.1063/1.470096

View online: <http://dx.doi.org/10.1063/1.470096>

View Table of Contents: <http://scitation.aip.org/content/aip/journal/jcp/103/2?ver=pdfcov>

Published by the [AIP Publishing](#)

---

### Articles you may be interested in

[Molecular-dynamics simulation of collisional energy transfer from vibrationally highly excited azulene in compressed CO<sub>2</sub>](#)

*J. Chem. Phys.* **108**, 10152 (1998); 10.1063/1.476474

[Collisional energy transfer between Ar and normal and vibrationally and rotationally frozen internally excited benzene-trajectory calculations](#)

*J. Chem. Phys.* **106**, 7080 (1997); 10.1063/1.473730

[Collisional energy transfer from highly vibrationally excited SF<sub>6</sub>](#)

*J. Chem. Phys.* **98**, 1034 (1993); 10.1063/1.464328

[Modeling collisional energy transfer in highly excited molecules](#)

*J. Chem. Phys.* **92**, 1819 (1990); 10.1063/1.458064

[Collisional energy transfer from highly vibrationally excited triatomic molecules](#)

*J. Chem. Phys.* **91**, 6804 (1989); 10.1063/1.457350

---



**NEW Special Topic Sections**

**NOW ONLINE**  
Lithium Niobate Properties and Applications:  
Reviews of Emerging Trends

**AIP** | Applied Physics  
Reviews

# Trajectory simulations of collisional energy transfer in highly excited benzene and hexafluorobenzene

Thomas Lenzer, Klaus Luther,<sup>a)</sup> and Jürgen Troe

*Institut für Physikalische Chemie, Universität Göttingen, Tammannstr. 6, D-37077 Göttingen, Germany*

Robert G. Gilbert

*School of Chemistry, University of Sydney, Sydney, New South Wales 2006, Australia*

Kieran F. Lim

*School of Chemistry, University of Melbourne, Parkville, Victoria 3052, Australia*

(Received 15 March 1995; accepted 31 March 1995)

Quasiclassical trajectory calculations of the energy transfer of highly vibrationally excited benzene and hexafluorobenzene (HFB) molecules colliding with helium, argon and xenon have been performed. Deactivation is found to be more efficient for HFB in accord with experiment. This effect is due to the greater number of low frequency vibrational modes in HFB. A correlation between the energy transfer parameters and the properties of the intramolecular potential is found. For benzene and HFB, average energies transferred per collision in the given energy range increase with energy. Besides weak collisions, more efficient “supercollisions” are also observed for all substrate–bath gas pairs. The histograms for vibrational energy transfer can be fitted by biexponential transition probabilities. Rotational energy transfer reveals similar trends for benzene and HFB. Cooling of rotationally hot ensembles is very efficient for both molecules. During the deactivation, the initially thermal rotational distribution heats up more strongly for argon or xenon as a collider, than for helium, leading to a quasi-steady-state in rotational energy after only a few collisions. © 1995 American Institute of Physics.

## I. INTRODUCTION

Collisional energy transfer (CET) between a highly excited molecule and a bath gas plays an important role in many fields of reaction dynamics. Although much effort has been expended over recent years,<sup>1–4</sup> detailed knowledge about this process in energetic regions relevant for chemical reactions is still lacking and the field is far from fully understood.

Most direct experiments on CET of polyatomic molecules have been focused on hydrocarbons and their substituted analogs like toluene- $h_8$  and  $-d_8$ ,<sup>5–10</sup> azulene- $h_8$  and  $-d_8$ ,<sup>11–17</sup> benzene- $h_6$  and  $-d_6$ ,<sup>10,18,19</sup> and hexafluorobenzene (HFB).<sup>20–24</sup> Quasiclassical trajectory calculations for azulene- $h_8$  and  $-d_8$ ,<sup>25–28</sup> and toluene- $h_8$  and  $-d_8$ ,<sup>29,30</sup> have been carried out to elucidate the fundamental mechanisms of CET (for a review see Gilbert<sup>31</sup>). The present article extends this series, reporting trajectory calculations for highly excited benzene and HFB molecules colliding with helium, argon, and xenon. As experimental studies of these two systems showed interesting differences, an analysis by classical trajectory calculations appeared particularly promising. The collisional deactivation of highly vibrationally excited benzene, prepared by internal conversion and detected by time-resolved infrared fluorescence (IRF) from C–H stretching modes was studied in Refs. 10, 18, and 19 at an initial excitation energy of about 40 700  $\text{cm}^{-1}$ . For noble gases like helium, argon and xenon, an approximately linear energetic dependence of the mean energy transferred per collision

$\langle \Delta E \rangle$  was found, with values of the order of  $-30 \text{ cm}^{-1}$  at the initial excitation energy. This is small in comparison to results for other aromatic hydrocarbons like toluene<sup>5,8</sup> and azulene.<sup>11,17</sup> The collisional relaxation of HFB, studied by the ultraviolet absorption (UVA) method,<sup>20</sup> on the other hand showed much higher values of  $\langle \Delta E \rangle$ . For example, HFB + argon at an energy of 30 000  $\text{cm}^{-1}$  has  $-330 \text{ cm}^{-1}$ , which is about a factor of 10 higher than for benzene + argon<sup>10,18</sup> and about a factor of 2 higher than for toluene + argon<sup>8</sup> (note that earlier UVA results for HFB<sup>21–24</sup> used an inadequate UVA calibration curve and should be reinterpreted). It appears of great interest to see whether classical trajectory calculations are able to reproduce and rationalize these observations and, hence, lead to a better understanding of the dominant “mechanisms” of energy transfer.

The calculations presented here are the first theoretical approach to study CET in these systems. Among other aspects we are also interested in the question whether “supercollisions,” i.e., collisions in which a large amount of energy is transferred, can be identified in these systems, and whether information can be gathered on their fraction and functional dependence on energy, etc. Steel *et al.*<sup>32</sup> have concluded from their “threshold experiments” that an appreciable fraction of supercollisions occurs in collisions involving vibrationally excited ground state HFB molecules and cyclobutene. Experiments carried out for highly excited toluene using detection by multiphoton ionization also support the presence of a small fraction of these highly efficient collisions.<sup>6</sup> The question remains open whether a small fraction of supercollisions can compete with the large majority of weak collisions.

<sup>a)</sup> Author to whom correspondence should be addressed.

## II. CHARACTERIZATION OF ENERGY TRANSFER

The highly excited polyatomic molecules considered in this study are characterized by a high density of states: typically  $(10^{10}-10^{30})/\text{cm}^{-1}$  at the energies of interest. No state-to-state specific energy transfer coefficients can be obtained under such conditions. CET in this quasicontinuum of rovibronic levels instead has to be characterized by energy-resolved rate coefficients  $R(E, E')$  in which a substrate molecule, with initial energy  $E'$ , undergoes a collision with a bath gas molecule and ends up with energy  $E$ . (In principle, the energy transfer should be characterized by the angular momentum  $J$  as well as the energy, since both are “good quantum numbers”, but no data on this angular momentum dependence are as yet available for large highly excited molecules.) In trajectory calculations,  $R(E, E')$  can be expressed as<sup>27</sup>

$$R(E, E') = \lim_{b_m \rightarrow \infty} \left( \frac{8k_B T}{\pi \mu} \right)^{1/2} \pi b_m^2 \int_0^\infty \int_0^{b_m} \frac{E_{\text{trans}}}{(k_B T)^2} \times \exp\left(-\frac{E_{\text{trans}}}{k_B T}\right) \frac{2\pi b}{\pi b_m^2} \times B(E, E'; E_{\text{trans}}, b) db dE_{\text{trans}}. \quad (1)$$

Here,  $b$  is the impact parameter,  $b_m$  is an effective hard-sphere diameter,  $E_{\text{trans}}$  is the relative impact energy and  $B(E, E'; E_{\text{trans}}, b)$  is the specific probability for energy transfer from energy  $E'$  to  $E$  for given initial values of  $E_{\text{trans}}$  and  $b$ . It is often convenient to express the rate coefficient  $R(E, E')$  with an energy transfer probability per collision  $P(E, E')$ :

$$R(E, E') = Z(E') P(E, E'), \quad (2)$$

where  $Z(E')$  is a reference collision number normally assumed to be energy independent. The Lennard-Jones (LJ) collision number used for this purpose is written as<sup>33</sup>

$$Z_{\text{LJ}} = \pi \sigma_{\text{LJ}}^2 \left( \frac{8k_B T}{\pi \mu} \right)^{1/2} \Omega^{(2,2)*}. \quad (3)$$

Here,  $\sigma_{\text{LJ}}$  is the LJ collision diameter and  $\Omega^{(2,2)*}$  is the relevant LJ collision integral.  $P(E, E')$  is normalized:

$$\int_0^\infty P(E, E') dE = 1 \quad (4)$$

and can be characterized by the moments of  $P(E, E')$ :

$$\langle \Delta E(E')^n \rangle = \int_0^\infty (E - E')^n P(E, E') dE = \frac{1}{Z} R_{E', n}, \quad (5)$$

where  $R_{E', n}$  are the moments of  $R(E, E')$ :

$$R_{E', n} = \int_0^\infty (E - E')^n R(E, E') dE. \quad (6)$$

Especially important are the first and second moments  $\langle \Delta E \rangle$ , the average energy transferred per collision, and  $\langle \Delta E^2 \rangle$ , the mean-squared-average energy transferred per collision. (Supercollisions can be characterized by the ratio  $\langle \Delta E^2 \rangle / \langle \Delta E \rangle^2$ .) An efficient basic method for obtaining the moments of  $R_{E', n}$  from classical trajectory calculations

evaluates Eqs. (1), (5), and (6) by fixing  $E'$  and choosing  $E_{\text{trans}}$  and  $b$  randomly from the appropriate distributions using Monte Carlo techniques. The moments  $R_{E', n}$  can then be obtained by<sup>27</sup>

$$R_{E', n} = \lim_{b_m \rightarrow \infty} \left( \frac{8k_B T}{\pi \mu} \right)^{1/2} \pi b_m^2 \lim_{N \rightarrow \infty} \frac{1}{N} \sum_{i=1}^N (\Delta E_i(b_m))^n. \quad (7)$$

Here,  $N$  is the number of trajectories used in the calculation. The trajectory averages  $\langle \Delta E^n \rangle_{\text{traj}}$  and the quantities  $\langle \Delta E^n \rangle$  deduced from experiment assuming a particular Lennard-Jones potential then are related by the ratio of the collision cross sections<sup>27</sup>

$$\langle \Delta E^n \rangle = \langle \Delta E^n \rangle_{\text{traj}} \frac{b_m^2}{\sigma_{\text{LJ}}^2 \Omega^{(2,2)*}}. \quad (8)$$

Additional information on the rotational dependence of  $R(E, E')$  is also desirable. In considering rotations, one has to note that, for a symmetric top with rotational energy:

$$E_{\text{rot}}(J, K) = BJ(J+1) + (A-B)K^2 \quad (9)$$

only  $J$  is a good quantum number while  $K$  is not necessarily conserved in the isolated molecule. Activating or deactivating the  $K$  rotor, therefore, may provide a gateway to changing the vibrational energy. In the present work we considered changes in  $J$  using a generalization<sup>30</sup> of the method of Schatz *et al.*<sup>34,35</sup> to nonlinear rotors. Rotational energy transfer was calculated via  $J$  from

$$\Delta E_{\text{rot}} = (AB^2)^{1/3} (J^2 - (J')^2), \quad (10)$$

where  $J'$  and  $J$  are the initial and final rotational states and  $(AB^2)^{1/3}$  is an effective rotational constant. Note that Eq. (10) makes the further approximation of a rigid spherical rotor, for ease of calculation: The effective rotational constant allows for the conversion between the rotational energy and  $J$  (which is exactly conserved before and after each collision).

## III. TRAJECTORY CALCULATIONS

### A. Intramolecular potential

Simple harmonic valence force fields (VFF) were used to describe both molecules, a type of potential frequently applied in trajectory calculations.<sup>25-30</sup> The total intramolecular potential consisted of contributions from harmonic stretches, bends, torsions and out-of-plane harmonic wags. Interactions between atoms not directly bonded to each other were assumed to be zero:

$$V_{\text{intra}} = \sum_i V_{\text{stretch}, i} + \sum_j V_{\text{bend}, j} + \sum_k V_{\text{torsion}, k} + \sum_l V_{\text{wag}, l}. \quad (11)$$

The individual terms of the total intramolecular potential have been defined before.<sup>28</sup> The equilibrium geometries were taken to be the same as those observed in experiment.<sup>36,37</sup> The diagonal force constants in Eq. (11) were initially taken to be the diagonal terms from Draeger's valence force field potentials for substituted benzene molecules,<sup>38</sup> and then var-

ied to give an optimal fit between our VFF frequencies and the experimental normal mode frequencies.<sup>36,39</sup> A summary of the potential parameters including the best fit final force constants together with a comparison between the normal mode frequencies predicted by the assumed intramolecular potential and the experimental frequencies can be found in Appendix A. Although this force field is highly simplified (as stated above, cross terms in the matrix of force constants are neglected), the mean deviation of the VFF frequencies from the experimental frequencies is only about 4% for benzene and 9% for HFB. One notices that the lower frequencies of some bends of HFB compared to benzene are well reproduced.

## B. Intermolecular potential

Knowledge of the detailed form of the intermolecular interaction potential is still poor, especially for larger systems. Trajectory calculations hitherto have often used interaction potentials which are sums of atom–atom LJ 12-6 or EXP-6 potentials obtained by more or less arbitrary combining rules.<sup>28</sup> No extensive experimental information exists on the noble gas+hydrocarbon or noble gas+fluorocarbon interaction potential, and nor are there detailed reliable quantum mechanical calculations. Differential cross section measurements<sup>40,41</sup> seem to provide some promise for obtaining more information in the future; however, even these cannot reveal the detailed interactions which are required for constructing the potential functions in trajectory calculations. For larger systems such experiments have been applied to the benzene+helium and pyridine+helium systems.<sup>42</sup> Theoretical approaches for describing non-bonding interactions between atoms<sup>43,44</sup> (which are tested in the calculations presented here) seem to be a first step to get access to more precise potential descriptions, but still use semiempirical combination rules.

In order to avoid this dilemma, as in former trajectory calculations,<sup>28</sup> the intermolecular potentials in this study at first was represented by a sum of pairwise atom–atom potentials

$$V_{\text{inter}} = \sum_i V_i. \quad (12)$$

For the atom–atom interactions three different types of intermolecular potentials have been used. The first was a LJ 12-6 potential with individual atom–atom terms given by

$$V = 4\epsilon_{X-M} \left[ \left( \frac{\sigma_{X-M}}{r} \right)^{12} - \left( \frac{\sigma_{X-M}}{r} \right)^6 \right] \quad (13)$$

(X=C,H,F; M=He,Ar,Xe), where  $r$  is the atom–atom center-of-mass separation and  $\epsilon_{X-M}$  and  $\sigma_{X-M}$  are the LJ well depth and radius, respectively, for the atom–atom interaction between a substrate atom X and the noble gas M. The parameters  $\epsilon_{X-M}$  and  $\sigma_{X-M}$  were calculated by the combination rules<sup>29</sup>

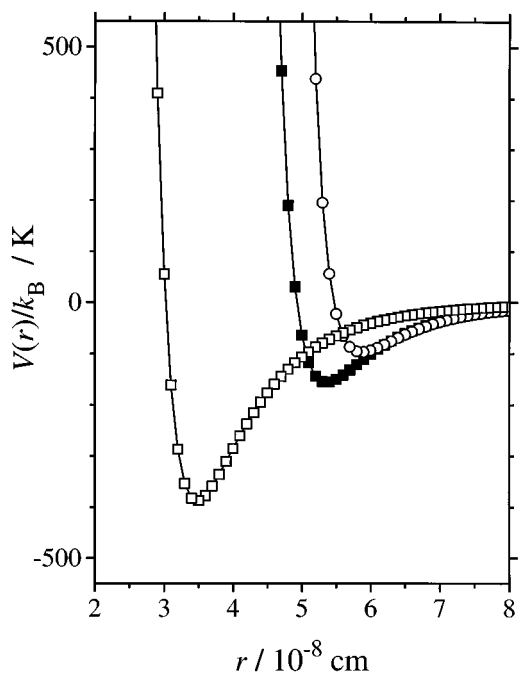


FIG. 1. LJ potential for an argon atom approaching a benzene molecule from different directions: ■ ( $x$  axis), ○ ( $y$  axis), □ ( $z$  axis); the potential is highly anisotropic; the  $z$  axis corresponds to the  $D_{6h}$  symmetry axis; the  $x$  and  $y$  axes are in the ring plane and are perpendicular to each other, the  $y$  axis being the axis which goes through two C–H bonds on opposite sides of the molecule.

$$\begin{aligned} \sigma_{H-M} &= \frac{1}{2}\lambda_1(\sigma_{\text{He}} + \sigma_M), & \epsilon_{H-M} &= \lambda_2\sqrt{\epsilon_{\text{He}}\epsilon_M}, \\ \sigma_{C-M} &= \frac{1}{2}\lambda_1(\sigma_{\text{Ne}} + \sigma_M), & \epsilon_{C-M} &= \lambda_2\sqrt{\epsilon_{\text{Ne}}\epsilon_M}, \\ \sigma_{F-M} &= \frac{1}{2}\lambda_1(\sigma_{\text{Ne}} + \sigma_M), & \epsilon_{F-M} &= \lambda_2\sqrt{\epsilon_{\text{Ne}}\epsilon_M}. \end{aligned} \quad (14)$$

The parameters  $\lambda_1$  and  $\lambda_2$  are fitted as described in Ref. 29 using the program SIGMON.<sup>45</sup> Note that Eq. (14) is different from our original prescription.<sup>28,45</sup>  $\lambda_1$  and  $\lambda_2$  were chosen so that the effective (=overall) molecular radius  $\sigma_{\text{eff}}$  and well depth  $\epsilon_{\text{eff}}$  were equal to the LJ radii and well depths calculated using the LJ parameters from Ref. 5; the following combination rules were used:

$$\sigma_{\text{eff},S-M} = \frac{1}{2}(\sigma_S + \sigma_M), \quad \epsilon_{\text{eff},S-M} = \sqrt{\epsilon_S\epsilon_M} \quad (15)$$

(S=benzene, HFB; M=He,Ar,Xe). Note that these LJ values differ slightly from the ones used in Ref. 10 for benzene+noble gas interactions but lead to nearly identical collision numbers. For a consistent comparison the experimental energy transfer parameters for benzene were rescaled to the collision numbers used in this paper. All relevant parameters for the intermolecular potentials can be found in Appendix B. Figure 1 shows the calculated model potential for the case of an argon atom approaching a benzene molecule from different directions. It can be seen that the potential is highly anisotropic, which is characteristic for all the potentials used in this study.

The second type of intermolecular potential used in this paper was an EXP-6 form in which the LJ  $r^{-12}$  repulsion is replaced by an exponential repulsion. In this case the atom–atom interaction is represented by

$$V = C_{X-M} \exp(-\eta_{X-M}r) - A4\epsilon_{X-M} \left( \frac{\sigma_{X-M}}{r} \right)^6 \quad (16)$$

( $X=C,H,F$ ;  $M=He,Ar$ ). The parameters  $C_{X-M}$  and  $\eta_{X-M}$ , which describe the exponential repulsion, were taken from theoretical first order Hartree–Fock SCF calculations in Ref. 44. For the attractive part two different sets of parameters were used. The first one was the same as in the LJ case with the scaling factor  $A$  equal to unity; the potential constructed in this way is called AHL-1. A second EXP-6 potential was obtained by simply scaling the factor  $A$  in the attractive part in such a way that the effective well depth  $\epsilon_{\text{eff}}$  between benzene/HFB and the noble gas was the same as in the LJ case. This type of potential is referred to as AHL-2. The LJ and AHL-2 potentials have the same effective well depths but a different shape of the repulsive wall. The parameters for these potentials can be found in Appendix B as well as their effective collision diameters  $\sigma_{\text{eff}}$  and well depths  $\epsilon_{\text{eff}}$ .

### C. Initial conditions and computational details

In the experiments corresponding to the present calculations, highly vibrationally excited molecules are prepared by laser excitation followed by internal conversion to the electronic ground state.<sup>8,10,20</sup> Angular momentum and total momentum are conserved during this excitation process such that a narrow, nearly microcanonical distribution of vibrationally hot but rotationally and translationally cold molecules is prepared initially. The selection of initial conditions for calculating trajectories corresponded to this excitation process:

(1) The initial translational distribution was chosen from a Boltzmann distribution at 300 K.

(2) The initial rotational distribution for the symmetric top molecules benzene and HFB was chosen from a thermal distribution at  $T_{\text{rot}}=300$  K (average rotational energy 313  $\text{cm}^{-1}$ ). For testing the influence of rotational energy transfer, rotational temperatures between 350 and 6000 K (corresponding to rotational energies between 365 and 6255  $\text{cm}^{-1}$ ) have also been used.

(3) The initial orientations of the excited molecules relative to the monoatomic collider were chosen by randomly rotating the molecules about their center of mass through the Euler angles.

(4) The initial vibrational phases and displacements were chosen from microcanonical ensembles at  $E'=53\,270$  (HFB), 40 700, 34 000, 24 000 or 14 000  $\text{cm}^{-1}$  (benzene and HFB). In all cases,  $E'$  is the initial energy in excess of the zero point energy.

(5) The initial impact parameter  $b$  was sampled randomly between 0 and a maximum value  $b_m$ . Reasonable choices for  $b_m$  were found by testing the convergence of the second moments  $R_{E',2}$  and  $R_{J',2}$  as a function of  $b$ . Maximum  $b_m$  values of 7 Å (helium), 8 Å (argon), and 10 Å (xenon) were sufficient in all cases to include the relevant

energy transfer events and were also low enough to omit elastic trajectories which do not contribute to the energy transfer.<sup>27,28</sup> It must be emphasized that the choice of a distinct  $b_m$  value has a direct influence on the height of the elastic peak of the transition probability  $P(E,E')$ . This point and its consequence for finding reasonable fits to  $P(E,E')$  will be discussed below.

The trajectories were calculated using a customized version of the computer program VENUS.<sup>46</sup> The selection of the initial conditions is a standard feature in this program. The initial center of mass separation was 13 Å and trajectories were terminated at a distance of 15 Å (measured between the rare gas atom and the closest atom in benzene/HFB).<sup>28</sup>

An integration step size of 0.1 fs (0.05 fs for the steepest potentials) was small enough to conserve the total energy to within  $\pm 0.1 \text{ cm}^{-1}$ . For benzene and HFB, 1000–3000 trajectories were calculated for each set of conditions (bath gas, intermolecular potential, and initial energy). The calculations were performed on Apollo DN 10000, DEC alpha 3000, and IBM RS/6000 workstations.

### D. Comparison of energy transfer parameters from trajectory calculations and experiments

All energy transfer parameters obtained from the trajectory calculations have been normalized to the reference collision numbers from Appendix B.

The IRF and UVA experiments used for comparison in this study are only sensitive to  $\langle\langle\Delta E(\langle E' \rangle)\rangle\rangle$ , the mean energy transferred per collision “bulk averaged” over the total population  $g$  at the mean energy  $\langle E' \rangle$ .<sup>47,48</sup> For narrow distributions of excited molecules far from thermal equilibrium one can assume (and this was tested<sup>49</sup>) that

$$\langle\Delta E(E')\rangle \approx \langle\langle\Delta E(\langle E' \rangle)\rangle\rangle \quad (17)$$

which allows a comparison of microcanonical  $\langle\Delta E\rangle$  values from trajectory calculations and bulk averaged  $\langle\langle\Delta E\rangle\rangle$  values from IRF and UVA experiments. The question arises as to the kind of energy has to be considered when comparing the IRF/UVA experimental and trajectory results: e.g., the vibrational energy  $E_{\text{vib}}$ , the total energy  $E_{\text{vib}}+E_{\text{rot}}$  of the excited molecule, or the energy of “active” modes. As will be shown in the next section, our results suggest that  $E'$  in Eq. (17) is the vibrational energy of the molecule for such experiments. In our case the rotational temperature of the molecules (in systems with sufficient coupling between the substrate and the bath gas) will have a slightly suprathreshold steady state value leading to  $\langle\Delta E_{\text{rot}}\rangle \approx 0$  during the deactivation.

Trajectory calculations also yield higher moments as  $\langle\Delta E^2\rangle$ , and these have been shown to be statistically more accurate than the corresponding  $\langle\Delta E\rangle$  values.<sup>29</sup> However, it must be kept in mind that the measured—and thus most important—quantity from IRF and UVA experiments is  $\langle\Delta E\rangle$ . For comparison it is possible to convert experimental IRF and UVA  $\langle\Delta E\rangle$  values into  $\langle\Delta E^2\rangle$  values using a distinct functional form for  $P(E,E')$ , e.g., an “exponential down model” with downward transitions given by

TABLE I. Comparison of  $\langle\Delta E\rangle$  and  $\langle\Delta E^2\rangle^{1/2}$  values for vibrational, rotational, and total energy transfer for benzene and HFB, collider gases: helium and argon,  $E'=24\,000\text{ cm}^{-1}$ , translational and rotational temperature 300 K, interaction potential: LJ 12-6; error limits are included.<sup>a</sup>

System	$\langle\Delta E_{\text{vib}}\rangle$ ( $\text{cm}^{-1}$ )	$\langle\Delta E_{\text{rot}}\rangle$ ( $\text{cm}^{-1}$ )	$\langle\Delta E_{\text{tot}}\rangle$ ( $\text{cm}^{-1}$ )	$\langle\Delta E\rangle$ (expt.) ( $\text{cm}^{-1}$ )
$\text{C}_6\text{H}_6$ +helium	$-91\pm 10$	$13\pm 10$	$-78\pm 17$	-27
$\text{C}_6\text{H}_6$ +argon	$-33\pm 5$	$26\pm 10$	$-7\pm 7$	-29
$\text{C}_6\text{F}_6$ +helium	$-201\pm 22$	$6\pm 5$	$-196\pm 22$	-170
$\text{C}_6\text{F}_6$ +argon	$-149\pm 9$	$38\pm 6$	$-111\pm 10$	-330

<sup>a</sup>Based on a bootstrap analysis as reported in Refs. 53–55.

$$P(E, E') = \frac{1}{N(E')} \exp\left(-\frac{(E' - E)}{\alpha(E')}\right), \quad E \leq E' \quad (18)$$

and upward transitions defined by “detailed balancing”:

$$P(E, E') = \frac{f(E)}{f(E')} P(E', E), \quad E \geq E', \quad (19)$$

where  $f(E)$  is the vibrational Boltzmann distribution

$$f(E) \propto \rho(E) \exp(-E/k_B T). \quad (20)$$

$\rho(E)$  is the density of vibrational quantum states at energy  $E$ .  $\alpha$  in Eq. (18) is fitted to the experimental values of  $\langle\Delta E\rangle$ , and from Eq. (5)  $\langle\Delta E^2\rangle$  can be readily evaluated. It must be kept in mind that this recipe for calculating “experimental”  $\langle\Delta E^2\rangle$  values may be not valid in all cases: The applied transformation depends on an arbitrary model of the transition probability. The detailed form of the transition probability for benzene and HFB has still to be extracted from appropriate experiments.<sup>6,19,50</sup>

## IV. RESULTS AND DISCUSSION

### A. Contributions of rotational and vibrational energy transfer for the colliders helium and argon

Calculations have been performed with regard to the partitioning of the total energy transfer ( $\langle\Delta E_{\text{tot}}\rangle$ ) into its rotational ( $\langle\Delta E_{\text{rot}}\rangle$ ) and vibrational ( $\langle\Delta E_{\text{vib}}\rangle$ ) contributions. Because of the larger mass of fluorine compared to hydrogen, the average moment of inertia around the three principal axes is larger by a factor of 5.5 for HFB than for benzene, which, for a given rotational energy, corresponds to a slower angular velocity. Together with the lower vibrational frequencies, a significant change in the collision dynamics may occur with HFB, which could be reflected by the amount of vibrational and rotational energy transferred. Calculations have been carried out for thermal and suprathermal rotational Boltzmann distributions. In Table I a comparison is given of the results for  $\langle\Delta E_{\text{vib}}\rangle$ ,  $\langle\Delta E_{\text{rot}}\rangle$  and  $\langle\Delta E_{\text{tot}}\rangle$  for benzene and HFB at vibrational energy  $E'=24\,000\text{ cm}^{-1}$  with argon as a collider and  $T_{\text{rot}}=300\text{ K}$ . The interaction potential was of LJ 12-6 type (see Appendix B). It can be seen that for the same bath gas  $\langle\Delta E_{\text{rot}}\rangle$  is small, positive and similar in size for both excited molecules. This means that the different values for total energy transfer are mainly determined by the different efficiencies in vibrational energy transfer (and thus by the size of  $\langle\Delta E_{\text{vib}}\rangle$ ). It can be seen that HFB is clearly more

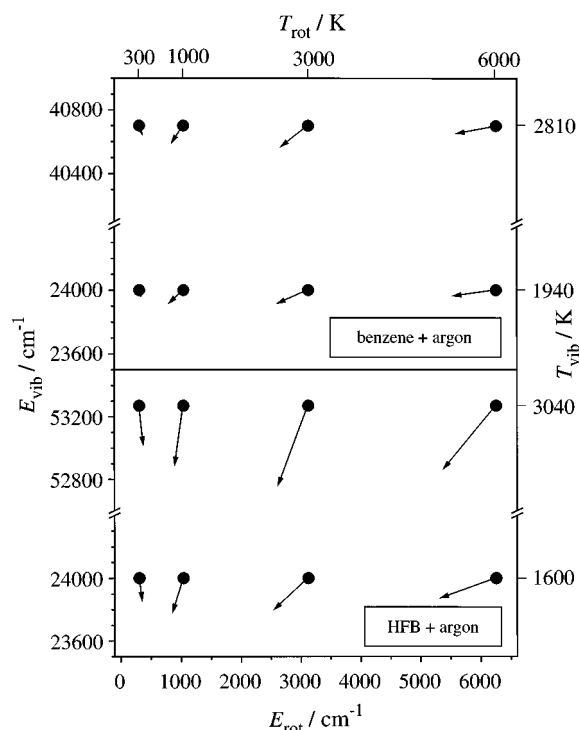


FIG. 2. Average flow of vibrational and rotational energy for eight different ensembles of excited benzene (upper plot) and HFB (lower plot) colliding with argon, interaction potential: LJ 12-6;  $E_{\text{vib}}=24\,000$  (benzene and HFB),  $40\,700$  (benzene) and  $53\,270\text{ cm}^{-1}$  (HFB);  $T_{\text{rot}}=300, 1000, 3000$  and  $6000\text{ K}$ ; the points (●) represent the initial state (microcanonical vibrational energy, mean rotational energy of the thermal ensemble) and the arrows represent the average rovibrational energy transferred (the arrow components correspond to  $\langle\Delta E_{\text{rot}}\rangle$  and  $\langle\Delta E_{\text{vib}}\rangle$  scaled to the reference collision numbers from Appendix B).

efficient than benzene. The heating up of the rotations is either caused by intramolecular  $V \leftrightarrow R$  energy redistribution or by the coupling with the bath gas during the close interaction. The differences in  $\langle\Delta E_{\text{rot}}\rangle$  between helium and argon may be due to the latter mechanism, because coupling will only play a minor or no role for shallow interaction wells but will be more efficient with increasing well depths of the overall potential. There appears to be a good correlation between the  $\epsilon_{\text{eff}}$  values and the extent of rotational heating due to a very weak coupling for helium but a more significant coupling for argon.

The results for  $T_{\text{trans}}=T_{\text{rot}}=300\text{ K}$  correspond to  $\Delta T_{\text{rot}}=14\text{ K}$  for benzene+helium,  $\Delta T_{\text{rot}}=6\text{ K}$  for HFB+helium,  $\Delta T_{\text{rot}}=27\text{ K}$  for benzene+argon and  $\Delta T_{\text{rot}}=40\text{ K}$  for HFB+argon. This is in very good agreement with the results from Ref. 30, where a value of  $\Delta T_{\text{rot}} \approx 0\text{ K}$  for toluene- $d_0$ +helium and  $\Delta T_{\text{rot}} \approx 30\text{ K}$  for toluene- $d_0$ +argon (LJ 12-6 potential) was found. The increasing CET efficiency from helium to argon is not correctly reproduced by the trajectory calculations. This is probably due to the choice of the parameters of the intermolecular LJ potential (see Sec. IV C). Thus the “correct” calculated absolute  $\langle\Delta E_{\text{vib}}\rangle$  and  $\langle\Delta E_{\text{rot}}\rangle$  values for “more realistic” helium interaction potentials would be even lower.

Figure 2 shows average flows in the vibrational–rotational energy plane. Each pair of initial vibrational and

rotational energies (microcanonical  $E_{\text{vib}}$ , canonical  $E_{\text{rot}}$ ) together with the arrow represent an average over a set of 1000 trajectories (3000 trajectories for the runs at 300 K). The following trends are observed:  $\langle \Delta E_{\text{rot}} \rangle$  is positive at low rotational temperatures ( $T_{\text{rot}}=300$  K). With increasing rotational temperature,  $\langle \Delta E_{\text{rot}} \rangle$  becomes negative ( $T_{\text{rot}}=1000$  K). For very high rotational temperatures  $\langle \Delta E_{\text{rot}} \rangle$  is strongly negative ( $T_{\text{rot}}=3000$  and 6000 K).  $\langle \Delta E_{\text{vib}} \rangle$  is always negative; the higher  $E_{\text{vib}}$ , the larger the absolute value of  $\langle \Delta E_{\text{vib}} \rangle$ . The absolute value of  $\langle \Delta E_{\text{vib}} \rangle$  appears to go through a maximum with increasing rotational temperature.

Our observations can be described most easily in terms of temperature differences between the translational, rotational and vibrational degrees of freedom. Because of the fact that, for both benzene and HFB,  $T_{\text{vib}}$  is much larger than  $T_{\text{trans}}$  there is always a loss of vibrational energy from benzene/HFB to argon caused by vibrational energy transfer ( $V \rightarrow T$  or  $V \rightarrow R \rightarrow T$ ). The amount of vibrational energy transfer depends on the difference between  $T_{\text{vib}}$  and  $T_{\text{trans}}$ . The positive value for  $\langle \Delta E_{\text{rot}} \rangle$  at  $T_{\text{rot}}=300$  K can be explained by intramolecular energy flow (depending on the difference between  $T_{\text{vib}}$  and  $T_{\text{rot}}$ ). For low rotational temperatures ( $T_{\text{rot}}=300$  K) there is an energy flow from the hot vibrations into the cold rotations which leads to a positive  $\langle \Delta E_{\text{rot}} \rangle$ . The fact that  $\langle \Delta E_{\text{rot}} \rangle$  is negative at high rotational temperatures can be explained by efficient  $R-T$  energy transfer from the hot rotations to the cold translation of argon, and also by intramolecular flow into the vibrations. Figure 2 suggests that the cooling of the rotations is very efficient, taking only about ten collisions even for the highest rotational temperatures, whereas the maximum vibrational energy loss per collision is about  $100 \text{ cm}^{-1}$  for benzene+argon and  $500 \text{ cm}^{-1}$  for HFB+argon. Similar trends were also observed in earlier trajectory calculations for the  $\text{SO}_2$ +argon system.<sup>51,52</sup> Our results suggest that after a few collisions a “quasi-steady-state” for the rotational temperature is achieved, in agreement with the work of Schatz *et al.*<sup>34,35</sup> In addition, we find a correlation that the higher the vibrational energy, the higher is the steady state  $T_{\text{rot}}$ . This is also important for the deactivation process as present in the experiments. Starting with an ensemble of vibrationally hot molecules with a rotational distribution of 300 K our results for argon show that a cascade of collisions (as present in IRF and UVA experiments) will—on average—heat up the rotations until a steady state value for  $T_{\text{rot}}$  will be reached. If one assumes that the rotational distributions during the deactivation can be approximately characterized by a canonical rotational temperature, the rotational steady state ( $\langle \Delta E_{\text{rot}} \rangle \approx 0$ ) can be found by varying the rotational temperature in our trajectory calculations. From Fig. 3 the approximate steady state value for  $T_{\text{rot}}$  at a vibrational energy of  $E'=24\,000 \text{ cm}^{-1}$  is about 395 K for benzene+argon and 415 K for HFB+argon. It is also demonstrated that, near to the steady state values of  $T_{\text{rot}}$ ,  $\langle \Delta E_{\text{vib}} \rangle$  is nearly independent on the rotational temperature. Further investigations showed that  $\langle \Delta E_{\text{vib}} \rangle$  is not sensitive to the shape of the rotational distribution. Even fixed microcanonical rotational temperatures between 300 and 450 K led to values for  $\langle \Delta E_{\text{vib}} \rangle$  which are similar to those of Table I and Fig. 3. In summary, the error

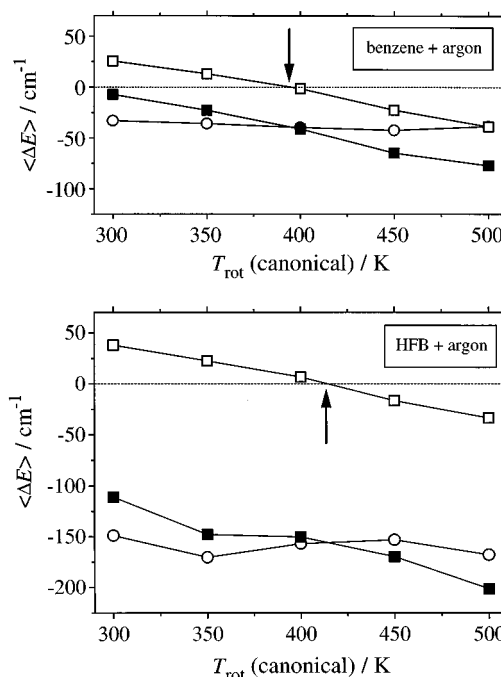


FIG. 3. Mean vibrational (○), rotational (□) and total (■) energy transferred per collision as a function of the average temperature for a canonical rotational Boltzmann distribution; upper plot: benzene+argon; lower plot: HFB+argon;  $E'=24\,000 \text{ cm}^{-1}$ , LJ 12-6 potential; the arrows indicate the region where the rotational steady state ( $\langle \Delta E_{\text{rot}} \rangle \approx 0$ ) is achieved; lines joining points are intended only as a guide for the eye and have no other significance.

for  $\langle \Delta E_{\text{vib}} \rangle$  introduced by using a rotational temperature which does not correspond exactly to the rotational temperature present in the experiment during the CET cascade, can be assumed to be small.

As a consequence  $\langle \Delta E_{\text{vib}} \rangle$  (and therefore also  $\langle \Delta E_{\text{vib}}^2 \rangle$ ) calculated from our type of trajectory calculations (which only investigate the first collision of a CET cascade) is the relevant quantity for the comparison with experiment, because it is—in contrast to  $\langle \Delta E_{\text{tot}} \rangle$ —not influenced by the intramolecular rotational heating process which is present in the first few collisions. CET is then purely transfer of vibrational energy via the  $V \rightarrow T$  pathway. When not otherwise stated in the following, energy transfer parameters without a subscript mean the vibrational quantities. The influence of rotational heating will be negligible in cases with only minor or no coupling: e.g., for helium (see Table I), where the steady state rotational temperature will only be slightly above or equal to 300 K (and thus  $\langle \Delta E_{\text{vib}} \rangle \approx \langle \Delta E_{\text{tot}} \rangle$ ).

Methods which directly calculate cascades of collisions<sup>34,35</sup> (and not an average over many single collisions) are an equally valid form of utilizing CET trajectory calculations, which can provide detailed information about the complete pathway during the deactivation including the exact rotational steady state distributions.

## B. Comparison of benzene and HFB energy transfer in collisions with argon

In order to examine the different behavior of benzene and HFB in CET experiments, trajectory calculations for ar-



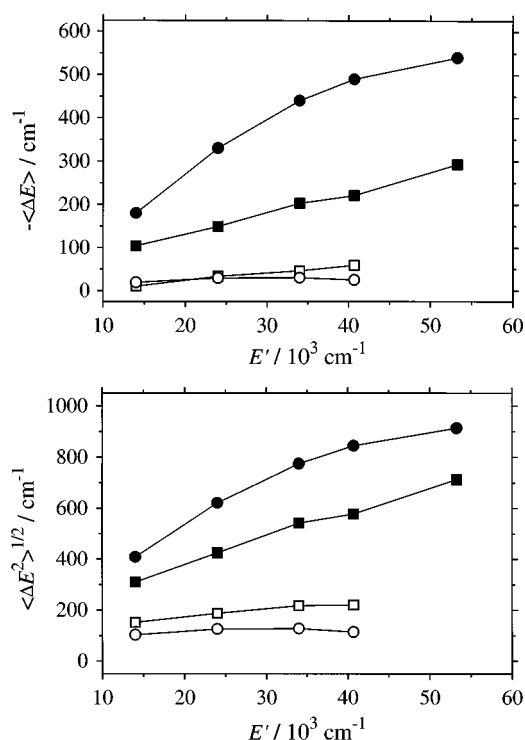


FIG. 4. Calculated and experimental energy transfer parameters  $\langle \Delta E \rangle$  and  $\langle \Delta E^2 \rangle^{1/2}$  as a function of the initial excitation energy  $E'$  for benzene and HFB; collider gas argon, LJ 12-6 interaction potential. ■ (HFB, trajectories), ● (HFB, experiment), □ (benzene, trajectories), ○ (benzene, experiment).

gon as bath gas were performed. Figure 4 shows the results for the first and second moments of energy transfer as a function of the initial vibrational energy of the excited molecule. For benzene and HFB  $-\langle \Delta E \rangle$  and  $\langle \Delta E^2 \rangle^{1/2}$  show an increase with energy. The experimental trend that both  $-\langle \Delta E \rangle$  and  $\langle \Delta E^2 \rangle^{1/2}$  are much higher for HFB compared to benzene is clearly reproduced but the absolute values show

some deviations. Possible reasons for the quantitative disagreement of some of the benzene and HFB results will be discussed below.

Calculations were performed in which single properties of the systems were changed independently. The CET behavior of the systems is determined by at least four characteristic quantities: the force constants, the geometry of the molecular framework, the masses of the atoms and the intermolecular potential parameters. In Table II the results for the different calculations are summarized as are energy transfer parameters for toluene for the Lennard-Jones potential.<sup>29</sup> Note that for reason of comparison with the toluene results from Ref. 29 the values for  $\langle \Delta E_{\text{tot}} \rangle$  and  $\langle \Delta E_{\text{tot}}^2 \rangle^{1/2}$  are also tabulated. Two different vibrational energies (24 000 and 40 700  $\text{cm}^{-1}$ ) were used. All energy transfer parameters have been scaled to the same LJ collision cross sections.

The calculations can be grouped as follows:

(1) Influence of the force constants: Introducing the HFB force constants (“F/B/B/B”) instead of the benzene ones (“B/B/B/B”) results in CET parameters nearly equal to the ones for  $\text{C}_6\text{H}_6$ . Note that the lowest vibrational frequencies are not significantly altered by this change of the force constants: Table III.

(2) Influence of the intermolecular potential parameters: Using the HFB intermolecular potential (B/F/B/B) instead of the one for benzene (B/B/B/B) also produces little change in the CET parameters. This is consistent with our earlier results<sup>29,30</sup> that CET scales roughly with the *effective* intermolecular well depth (Appendix B).

(3) Influence of the geometry: Comparison of B/B/B/B and B/B/F/B shows an increase in  $-\langle \Delta E \rangle$  and  $\langle \Delta E^2 \rangle^{1/2}$  at 40 700 and 24 000  $\text{cm}^{-1}$  (note that there is no change in  $\langle \Delta E_{\text{tot}}^2 \rangle^{1/2}$  at 24 000  $\text{cm}^{-1}$ , which can be explained by the influence of the rotational contribution which dominates the trend in  $\langle \Delta E_{\text{vib}}^2 \rangle^{1/2}$ ). Comparison of B/B/B/F and B/B/F/F also shows a change in  $\langle \Delta E \rangle$  and  $\langle \Delta E^2 \rangle^{1/2}$  at both energies. Minor deviations of individual values are due to the statistical errors of the trajectory calculations, which are quantified

TABLE II. Influence of a change of force constants, intermolecular potential, geometry and masses on  $\langle \Delta E \rangle$  and  $\langle \Delta E^2 \rangle^{1/2}$  for highly excited benzene, HFB, perdeuterobenzene, toluene and perdeuterotoluene colliding with argon.  $T_{\text{trans}} = T_{\text{rot}} = 300$  K; LJ 12-6 interaction potential reference collision cross section:  $0.846 \cdot 10^{-14}$   $\text{cm}^2$ ; abbreviations: B=benzene, F=HFB and D=perdeuterobenzene.<sup>a</sup>

System (force constants/ intermolecular potential/ geometry/masses)	$E' = 24\,000 \text{ cm}^{-1}$				$E' = 40\,700 \text{ cm}^{-1}$			
	$-\langle \Delta E \rangle (\text{cm}^{-1})$		$\langle \Delta E^2 \rangle^{1/2} (\text{cm}^{-1})$		$-\langle \Delta E \rangle (\text{cm}^{-1})$		$\langle \Delta E^2 \rangle^{1/2} (\text{cm}^{-1})$	
	Vib.	Tot.	Vib.	Tot.	Vib.	Tot.	Vib.	Tot.
$\text{C}_6\text{H}_6$ (B/B/B/B)	$33 \pm 5$	$7 \pm 7$	$187 \pm 10$	$270 \pm 9$	$59 \pm 5$	$21 \pm 6$	$220 \pm 11$	$276 \pm 8$
(F/B/B/B)	$23 \pm 9$	$0 \pm 11$	$178 \pm 16$	$240 \pm 11$	$62 \pm 12$	$23 \pm 13$	$240 \pm 28$	$262 \pm 13$
(B/F/B/B)	$39 \pm 10$	$11 \pm 12$	$189 \pm 12$	$272 \pm 15$	$70 \pm 11$	$36 \pm 13$	$234 \pm 16$	$287 \pm 15$
(B/B/F/B)	$59 \pm 6$	$38 \pm 7$	$221 \pm 11$	$267 \pm 8$	$105 \pm 8$	$67 \pm 8$	$294 \pm 14$	$302 \pm 11$
(B/B/B/F)	$106 \pm 9$	$81 \pm 9$	$326 \pm 23$	$346 \pm 19$	$188 \pm 23$	$149 \pm 22$	$482 \pm 49$	$464 \pm 39$
(B/B/F/F)	$143 \pm 19$	$115 \pm 19$	$427 \pm 46$	$403 \pm 31$	$222 \pm 27$	$183 \pm 25$	$562 \pm 63$	$515 \pm 36$
$\text{C}_6\text{F}_6$ (F/F/F/F)	$167 \pm 10$	$124 \pm 11$	$448 \pm 21$	$446 \pm 21$	$248 \pm 13$	$190 \pm 12$	$611 \pm 36$	$547 \pm 31$
$\text{C}_6\text{D}_6$ (B/B/B/D)	$45 \pm 8$	$19 \pm 10$	$180 \pm 10$	$253 \pm 12$	$61 \pm 9$	$21 \pm 12$	$227 \pm 15$	$282 \pm 14$
Toluene- $d_0$	...	$38 \pm 20$	...	$287 \pm 31$	...	$140 \pm 28$	...	$415 \pm 52$
Toluene- $d_8$	...	$69 \pm 24$	...	$344 \pm 37$	...	$177 \pm 33$	...	$491 \pm 79$

<sup>a</sup>Toluene/perdeuterotoluene: results from Ref. 29; excitation energy 41 000 instead of 40 700  $\text{cm}^{-1}$ ; results at  $E' = 24\,000 \text{ cm}^{-1}$  interpolated.

TABLE III. Influence of a change of force constants, geometry, and masses on the lowest valence force field (VFF) vibrational frequencies for benzene, HFB, perdeuterobenzene, toluene and perdeuterotoluene.<sup>a</sup> The 12 ( $3N_{\text{ring}}-6$ ) lowest frequencies are taken for comparison; frequencies are in ascending order; abbreviations: B=benzene, F=HFB and D=perdeuterobenzene.

System (force constants/intermolecular potential/geometry/masses)	Lowest VFF vibrational frequencies ( $\text{cm}^{-1}$ )											
$\text{C}_6\text{H}_6$ (B/B/B/B)	400	400	617	617	657	680	833	833	926	991	991	1015
(F/B/B/B)	400	400	657	680	713	713	833	833	867	1015	1015	1018
(B/F/B/B)	400	400	617	617	657	680	833	833	926	991	991	1015
(B/B/F/B)	370	370	555	601	617	617	713	713	879	879	897	897
(B/B/B/F)	145	145	198	242	270	270	276	291	291	377	377	417
(B/B/F/F)	126	126	172	197	223	223	227	245	245	245	378	378
$\text{C}_6\text{F}_6$ (F/F/F/F)	126	126	172	197	271	271	278	285	285	379	379	444
$\text{C}_6\text{D}_6$ (B/B/B/D)	351	351	499	550	596	596	648	648	772	772	819	819
Toluene- $d_0$	195	329	346	448	496	605	616	766	865	946	957	976
Toluene- $d_8$	172	287	293	378	458	493	594	653	703	755	790	793

<sup>a</sup>Toluene and perdeuterotoluene frequencies from the VFF used in Ref. 29.

in Table II by bootstrap estimates.<sup>53–55</sup> However, the effect of changing from a benzene geometry to a HFB geometry is significantly smaller than the effect of perfluorination.

(4) Influence of perfluorination and perdeuteration. CET values similar to the ones for  $\text{C}_6\text{F}_6$  (F/F/F/F) are obtained when changing masses (i.e., substituting  $^1\text{H}$  by an artificial  $^{19}\text{H}$  having fluorine mass: B/B/B/F). This change also leads to switching from a weak to a stronger energetic dependence of the energy transfer parameters. These effects both have an influence on the vibrational and total energy transfer. The increase in CET is consistent with perdeuteration effects in Table II ( $\text{C}_6\text{D}_6+\text{Ar}$ : B/B/B/D) and in other studies by ourselves<sup>26,29,30</sup> and other workers. This is discussed further below.

It can be concluded that the differences in benzene and HFB energy transfer are mainly caused by the mass change. Furthermore, the observed changes in CET behavior for all calculations are directly correlated with the distribution of the normal mode vibrational frequencies. The increase of mass from substituting hydrogen by fluorine (B/B/B/F) leads to a pronounced decrease in the frequencies of the normal modes, especially the low frequencies which are thought to govern CET: it has been suggested<sup>25</sup> that this is due to low frequencies causing the chattering interactions that characterize energy transfer in polyatomics to “linger longer” and thus transfer more energy. This latter supposition is consistent with the large jump in CET efficiency found for the B/B/B/F calculation. Changing both, mass and geometry together (B/B/F/F), leads to a further decrease of the lowest frequencies, which are nearly identical to the ones for the F/F/F/F force field, and the energy transfer parameters for both calculations are identical within the error limits. This correlation can be extended to other molecules similar to benzene, e.g., perdeuterobenzene, toluene and perdeuterotoluene. In the case of deuteration, the change in the vibrational frequencies, and therefore in  $\langle\Delta E\rangle$  and  $\langle\Delta E^2\rangle^{1/2}$ , is much smaller, because of the smaller mass effect compared to fluorination. A small increase in energy transfer efficiency is found in the results for perdeuterobenzene, where the frequency distribution as well as the values for  $\langle\Delta E\rangle$  and  $\langle\Delta E^2\rangle^{1/2}$  for perdeuterobenzene are similar to the one for the

B/B/F/B calculation (Tables II and III). The reasons for this small effect have been discussed by Clarke *et al.*<sup>26</sup> by deuteration, the CH stretching frequencies and to a lesser extent the CH bending modes change the most (decreasing by a factor of  $2^{-1/2}$ ) while the low-frequency modes are relatively unchanged. If one assumes that CET is primarily governed by the low-frequency modes, the small deuteration effect seems reasonable. In contrast, with perfluorination the higher-frequency modes involved in the CH stretching and bending are completely removed (see Appendix A and Table III), creating many more normal modes having extremely low frequencies. Correspondingly, the amount of energy transferred is clearly increased.

The values for toluene- $d_0$ +argon and toluene- $d_8$ +argon are also given in Tables II and III; these are the results for total energy transfer for the Lennard-Jones potential termed “ $t$ -Ar5” in Ref. 29. Note that the energy transfer parameters are only approximate, because they had to be interpolated from the “toluene+ $^4\text{Ar}$ ” and “toluene+ $^{40}\text{Ar}$ ” data sets. From the frequency distribution one would assume that  $\langle\Delta E\rangle$  and  $\langle\Delta E^2\rangle^{1/2}$  should lie between the values of the B/B/F/B and B/B/B/F results—and (within the error limits) this is indeed the case: at  $24\,000\text{ cm}^{-1}$   $-\langle\Delta E\rangle$  and  $\langle\Delta E^2\rangle^{1/2}$  are slightly higher than for the B/B/F/B run and at about  $41\,000\text{ cm}^{-1}$  slightly lower than for the B/B/B/F run. For toluene- $d_8$ <sup>29</sup> the effect of deuteration on the frequency distribution and the energy transfer parameters is also visible and more pronounced than for benzene- $d_8$ . Similar trends have been observed in trajectory calculations for azulene- $h_8$  and the deuterated species azulene- $d_8$ .<sup>26</sup>

Finally, it should be noted that our results are consistent with simple treatments for  $V\rightarrow T$  energy transfer between diatomic molecules and atoms, for example: Both the Landau–Teller<sup>56</sup> and SSH theories<sup>57,58</sup> predict a more efficient energy transfer for vibrational modes having lower frequencies. Our data suggest that the results of these simple models are also valid for polyatomic systems with many coupled oscillators. The extreme drop of the normal mode frequencies and completely different character of the frequency distribution of HFB leads to an enhanced CET compared to benzene/toluene or other hydrocarbons. This shows

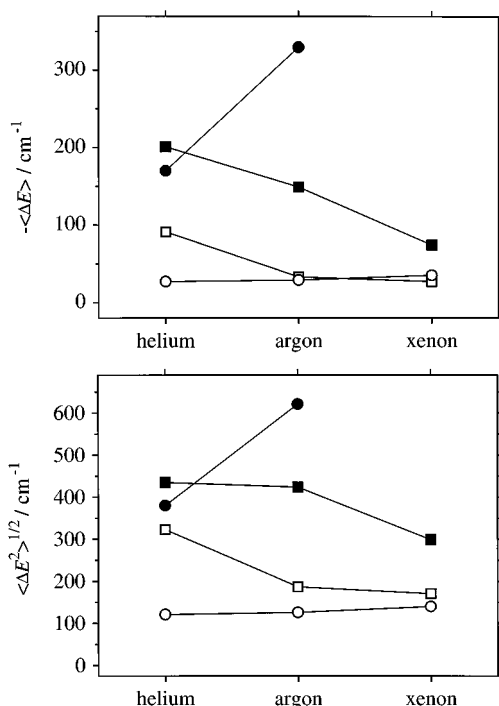


FIG. 5.  $\langle \Delta E \rangle$  and  $\langle \Delta E^2 \rangle^{1/2}$  for benzene and HFB as a function of bath gas; translational and rotational temperature 300 K,  $E' = 24\,000\text{ cm}^{-1}$ , LJ 12-6 potential; ■ (HFB, trajectories), ● (HFB, experiment), □ (benzene, trajectories), ○ (benzene, experiment).

that the correct frequency spectrum is needed to reproduce the CET trends in trajectory calculations.

### C. Dependence of energy transfer parameters on bath gas and intermolecular potential

#### 1. LJ 12-6 potential

Calculations for the bath gases helium, argon, and xenon were performed using a sum of pairwise LJ 12-6 potentials as described in Sec. III B. Plots for  $\langle \Delta E \rangle$  and  $\langle \Delta E^2 \rangle^{1/2}$  as a function of bath gas are presented in Fig. 5. The values are for an excitation energy of  $24\,000\text{ cm}^{-1}$ . All experimental and calculated values for a given bath gas were scaled to correspond to the same LJ collision number (Appendix B). The calculations at the other excitation energies lead to very similar trends. For all the bath gases the experimental observation that fluorination increases  $-\langle \Delta E \rangle$  and  $\langle \Delta E^2 \rangle^{1/2}$  is qualitatively reproduced. However, the absolute values show some deviations. In the benzene case the agreement for  $\langle \Delta E \rangle$  is very good for argon and xenon whereas the calculated  $\langle \Delta E^2 \rangle^{1/2}$  values are slightly higher. This means that the shape of the vibrational transition probabilities from trajectories for these bath gases cannot be purely monoexponential as assumed in the transformation of the experimental  $\langle \Delta E \rangle$  values. Thus a final judgement of the  $\langle \Delta E^2 \rangle^{1/2}$  values from trajectory calculations will only be possible if experimental data on the shape of the transition probability become available in the future. For benzene+helium, the energy transfer parameters are consistently too high (see below). For HFB the agreement for helium as a collider is good (the calculated  $\langle \Delta E \rangle$  and  $\langle \Delta E^2 \rangle^{1/2}$  values being slightly too high) whereas

for argon the calculated energy transfer parameters are too low. From helium to xenon the experimental  $-\langle \Delta E \rangle$  and  $\langle \Delta E^2 \rangle^{1/2}$  values are increasing whereas for the trajectory values the opposite trend is observed. Some trajectory studies which investigated the variation of energy transfer with systematic variation of the bath gas also observed this decreasing trend for the systems  $\text{CS}_2 + \text{helium/argon/xenon}$ <sup>34,35</sup> and azulene+helium/argon/xenon.<sup>27,28</sup> In the case of  $\text{CS}_2$ , the trend agrees with experiment whereas for azulene the trajectories show the wrong trend (similar to the situation for benzene and HFB). The deviations from the experimental values in the azulene case were thought to be caused by the lack of knowledge of the exact form of the intermolecular potential especially for the light bath gas helium. Calculated values for  $\langle \Delta E^2 \rangle^{1/2}$  being three times higher than the experimental values was ascribed to the model potential having too steep a repulsive wall. Recent calculations for the systems toluene+helium/argon<sup>29</sup> also come to the conclusion that the repulsive part of the potential predominantly determines the amount of energy transferred, and it is proposed that the effective well depth of the overall potential can play a role in some cases (see below). In addition, these calculations suggest that some of the differences between trajectories and experiment for the change of CET with bath gas are most probably due to the method of choosing the parameters of the intermolecular potential. In these calculations it was shown that different semiempirical “recipes” for setting up the intermolecular potential, especially the use of slightly different potential parameters for the local atom–atom interactions, can better reproduce the correct trend with bath gas. Later in this section it will also become clear that the specific functional form of the transition probabilities found in the trajectory calculations can explain some of the differences especially in  $\langle \Delta E^2 \rangle^{1/2}$ . It will emerge that a monoexponential form for  $P(E, E')$  does not lead to an adequate description of the trajectory results (as was assumed for the transformation of the experimental  $\langle \Delta E \rangle$  values in Figs. 4 and 5) and that a biexponential form can be used for a reasonable fit.

#### 2. EXP-6 potential

Ahlich and co-workers have calculated potential parameters for exponential repulsive interactions between atoms.<sup>44</sup> The parameters  $C_{X-M}$  and  $\eta_{X-M}$  [see Eq. (16)] were determined using a first order SCF Hartree–Fock method. In our study their values for helium, argon, carbon, hydrogen, and fluorine were used to construct the repulsive part of the model potential. Their parameters for benzene/HFB+helium/argon can be found in Appendix B. For the AHL-1 potential the attractive  $r^{-6}$  part was the same as in the LJ case. For the AHL-2 potential the parameters for the attractive part were scaled as discussed in Sec. III B. Figure 6 shows a comparison between the LJ 12-6, AHL-1, and AHL-2 potentials for benzene+helium with helium approaching from the  $z$  axis of benzene. Compared with the LJ potential, the AHL-1 potential has a softer repulsive wall and the well is shallower. The AHL-2 potential has the same “repulsive terms” as the AHL-1 potential but its effective well depth is identical to the LJ potential.

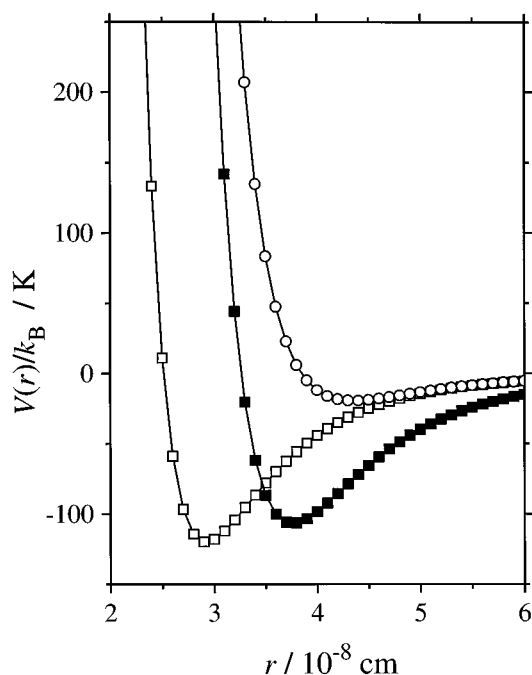


FIG. 6. Comparison between the LJ 12-6 (□), AHL-1 (○) and AHL-2 (■) potential for benzene+helium for an approach of the noble gas atom from the  $z$  direction (axes definition as for Fig. 1).

Energy transfer parameters for benzene+helium/argon and HFB+helium/argon, calculated using the LJ 12-6 and EXP-6 potential forms described above, are compared with the experimental values in Table IV. The  $\langle \Delta E \rangle$  and  $\langle \Delta E^2 \rangle^{1/2}$  values were scaled with the LJ collision numbers from Appendix B. Obviously, the absolute values of the energy transfer parameters are smaller for the exponential repulsion than for the  $r^{-12}$  repulsion. For the helium and argon case both the benzene and HFB energy transfer efficiency obtained for the AHL-2 potential is slightly higher than for the AHL-1 potential and the absolute values of  $\langle \Delta E \rangle$  and  $\langle \Delta E^2 \rangle^{1/2}$  are significantly lower than for the LJ case.

This is in accord with other studies<sup>29,30,35</sup> which have shown that the steepness of the repulsive term has a direct effect on the magnitude of CET. Furthermore, it turns out that the values for the EXP-6 potential with the deeper well

(AHL-2) are higher than for the system with the shallow well (AHL-1). However, a more detailed comparison of the AHL-1 and AHL-2 potential cannot be made since both  $\sigma_{\text{eff}}$  and  $\epsilon_{\text{eff}}$  are different, but it is interesting that the same trend has also been observed in calculations for the toluene+helium/argon systems.<sup>29</sup> For benzene+helium, the collision is not affected by the presence of the well since the trajectories are sampling the repulsive wall (this can be described as an “impulsive collision”). In this case the attractive part in the potential represents a small perturbation of the repulsive potential and removal of this potential term has no significant effect on CET.<sup>35</sup> However, for sufficiently deep wells (e.g., for benzene+argon), CET is increased. In these cases the collision lifetime is longer.<sup>29</sup> This leads to a greater likelihood of redistribution of energy among the degrees of freedom of both collision partners (and to more coupling during the interaction as described in Sec. IV A).

None of the EXP-6 potentials presented here gives a completely satisfactory description of the experimental CET. The EXP-6 potentials show a “better” but still not correct bath gas dependence in  $\langle \Delta E^2 \rangle^{1/2}$  and  $\langle \Delta E \rangle$  when compared to the LJ potential. The absolute  $\langle \Delta E \rangle$  values from trajectories are nearly correct for benzene+helium (which is a significant improvement compared to the values for the LJ potential) but too small for benzene+argon and HFB+helium/argon. The  $\langle \Delta E^2 \rangle^{1/2}$  values are in agreement within 20%–40% for benzene+helium/argon and too small for HFB+helium/argon. Part of the differences, especially for  $\langle \Delta E^2 \rangle^{1/2}$ , is probably due to the form of the trajectory transition probabilities which are not monoexponential.

Finally, it must be emphasized again that both the LJ and EXP-6 potentials used here are only model potentials based on physically reasonable assumptions and combination rules. Another reason for the disagreement with experiment may be caused by the presence of quantum effects, as discussed in Ref. 59. However, one of the most important factors is surely that precise experimental or theoretical potential data, including knowledge of the exact atom–atom interactions, together with more sophisticated combining rules for experimentally inaccessible systems, are a basic requirement to obtain quantitative agreement.

TABLE IV. Comparison of the root-mean-squared and average vibrational energies transferred per collision for highly excited benzene and HFB using different forms of the intermolecular potential; collider gases helium and argon,  $E' = 24\,000\text{ cm}^{-1}$ , rotational and translational temperature 300 K. The parameters for the LJ 12-6, AHL-1 and AHL-2 potentials can be found in Appendix B.

System	Helium		Argon	
	$\langle \Delta E \rangle$ (cm <sup>-1</sup> )	$\langle \Delta E^2 \rangle^{1/2}$ (cm <sup>-1</sup> )	$\langle \Delta E \rangle$ (cm <sup>-1</sup> )	$\langle \Delta E^2 \rangle^{1/2}$ (cm <sup>-1</sup> )
C <sub>6</sub> H <sub>6</sub> (LJ 12-6)	-91	323	-33	187
C <sub>6</sub> H <sub>6</sub> (AHL-1)	-10	119	-1	74
C <sub>6</sub> H <sub>6</sub> (AHL-2)	-16	138	-3	102
C <sub>6</sub> H <sub>6</sub> (experiment)	-27	121	-29	126
C <sub>6</sub> F <sub>6</sub> (LJ 12-6)	-201	435	-149	424
C <sub>6</sub> F <sub>6</sub> (AHL-1)	-84	237	-68	235
C <sub>6</sub> F <sub>6</sub> (AHL-2)	-100	260	-99	292
C <sub>6</sub> F <sub>6</sub> (experiment)	-170	380	-330	621

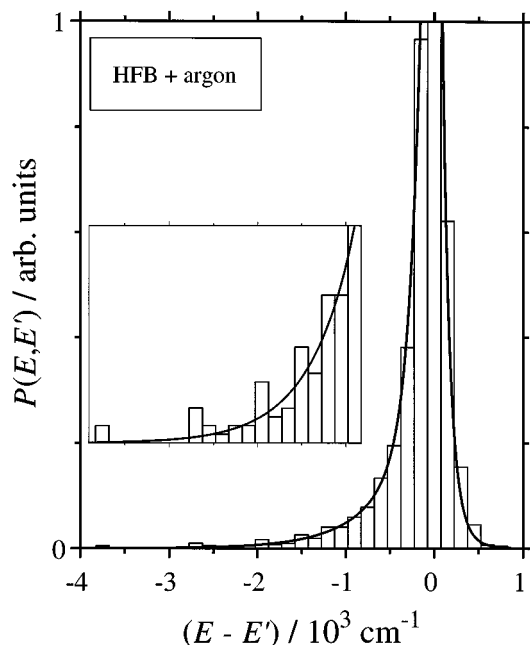


FIG. 7.  $P(E, E')$  histogram for vibrational energy transfer in the system HFB+argon,  $E'=24\,000\text{ cm}^{-1}$ , translational and rotational temperature 300 K, LJ 12-6 interaction potential; the solid line is the best biexponential fit from a Levenberg–Marquardt algorithm as described in the text; the elastic peak is truncated.

## D. Supercollisions

### 1. Transition probabilities deduced from trajectory data

Collisions in which large amounts of energy are transferred are commonly termed as “strong collisions” or “supercollisions.” Their occurrence has been observed both in experiments<sup>6,32</sup> and in trajectory calculations.<sup>60–62</sup> Supercollisions are also found in our trajectory calculations. In order to quantify this phenomenon, trajectory calculations for benzene and HFB were performed using up to 3000 trajectories. Figure 7 shows a  $P(E, E')$  histogram of vibrational energy transfer for HFB+argon. It can be seen that in most of the collisions only small amounts of energy are transferred. Supercollisions are relatively rare and appear as energy transfer events in the tail of the histogram for large amounts of transferred energy.

Many attempts have been made over the last years to obtain realistic fits for these transition probabilities. There is the well known problem of incorporating the elastic peak in such a fitting procedure. One way is simply to omit the elastic collisions, but this introduces an arbitrariness, as the truly elastic collisions ( $E=E'$ ) of course are of “measure zero” in  $P(E, E')$ . Thus the fits to the transition probabilities can be much dependent on the choice of the histogram grain size for removing the elastic peak. To deal with this problem various approaches have been taken: e.g., Schatz *et al.* took a grain size of about  $\langle \Delta E \rangle$  and fitted only the wings of the trajectory distribution as the sum of two exponential model functions.<sup>62</sup> Troe *et al.* fitted the wings of the transition probability by a monoexponential model function and included the grain size as an additional parameter in a least squares fitting

procedure.<sup>51,52</sup> Two objectives were used to determine the fitting method in the present paper. First, simple functional forms, in this case a biexponential, were used to fit the  $P(E, E')$  results. At the given level of statistical uncertainty in the “far wing” of the  $P(E, E')$  trajectory histograms, precise quantitative inferences on the functional form of the supercollision component of  $P(E, E')$  cannot yet be made, and hence the reasonably accurate fitting with simple biexponentials does not imply that the choice of this functional form is shown to be unique. However, this type of fitting provides a good basis for meaningful comparisons with other calculations<sup>51,52,62</sup> and with experimental  $P(E, E')$ .<sup>50</sup> Note that fitting with a biexponential form implies that the elastic peak has been excluded. Second, the arbitrariness of the width chosen for the elastic peak can be obviated by testing for the effect its omission has on the observable in question. Thus master equation calculations show that the most inefficient collisions ( $E \text{ approximately } = E'$ ) do not make any significant contributions to, e.g., the resulting energy flow in collisional deactivation, energy transfer moments like  $\langle \Delta E \rangle$ , or falloff curves. Hence one could determine the width of the elastic peak by requiring that exclusion of the elastic peak so defined does not significantly change the calculated experimental observable. In the present case we could show that there is a large range of grain size which satisfies this criterion. In addition, weighting is used to adjust the required fitting accuracy according to the relative importance of energy transfer at various  $(E - E')$  values for resulting experimental observables, like  $\langle \Delta E \rangle$ , in multicollisional processes. Specifically, as a suitable functional form we write, as in Ref. 63,

$$P(E, E') = \frac{1}{N} \left[ (1-x) \cdot \exp\left(-\frac{(E'-E)}{\alpha}\right) + x \cdot \exp\left(-\frac{(E'-E)}{\gamma}\right) \right], \quad E \leq E', \quad (21)$$

where  $\alpha$  can be seen as  $\langle \Delta E_{\text{down}} \rangle$  for the weak collision part of the transition probability, whereas  $\gamma$  is  $\langle \Delta E_{\text{down}} \rangle$  for the supercollision part.  $x$  is a weighting factor for the supercollision component and  $N$  is a normalization constant for obeying Eq. (4). For the upward half an analogous definition is used:

$$P(E, E') = \frac{1}{N} \left[ (1-x) \cdot \exp\left(-\frac{(E-E')}{\beta}\right) + x \cdot \exp\left(-\frac{(E-E')}{\delta}\right) \right], \quad E \geq E'. \quad (22)$$

The downward and upward half of each histogram are fitted simultaneously with detailed balance directly included in the fitting routine. This is approximately fulfilled by relating  $\alpha$  and  $\beta$ , as well as  $\gamma$  and  $\delta$ , through<sup>63</sup>

$$\begin{aligned} \beta &\approx \alpha F_E k_B T / (\alpha + F_E k_B T), \\ \delta &\approx \gamma F_E k_B T / (\gamma + F_E k_B T), \end{aligned} \quad (23)$$

where the factor  $F_E$  has a value, which—in our case—is very close to unity. This restriction of the fit has the advantage that—despite smaller statistical errors in the histogram

TABLE V. Fitted parameters for the downward wing of the vibrational transition probabilities for benzene and HFB colliding with helium, argon, and xenon at the vibrational energy  $E' = 24\,000\text{ cm}^{-1}$ ; the rotational energies for the trajectory sets were selected from thermal Boltzmann distributions at 300 K, interaction potential: LJ 12-6.

System	$x$ (%)	$\alpha$ ( $\text{cm}^{-1}$ )	$\gamma$ ( $\text{cm}^{-1}$ )
$\text{C}_6\text{H}_6 + \text{helium}$	14	87	313
$\text{C}_6\text{H}_6 + \text{argon}$	9	68	223
$\text{C}_6\text{H}_6 + \text{xenon}$	3	85	241
$\text{C}_6\text{F}_6 + \text{helium}$	40	108	352
$\text{C}_6\text{F}_6 + \text{argon}$	11	120	509
$\text{C}_6\text{F}_6 + \text{xenon}$	1	121	962

distributions—detailed balance is fulfilled in every case. A Levenberg–Marquardt algorithm implemented in the fitting routine<sup>64</sup> was used to determine the parameters  $\alpha$ ,  $\gamma$ , and  $x$  of the transition probability. For the fitting procedure the elastic peak is omitted. There is of course the question of the energy grain employed to subdivide the trajectory histogram or—equivalently—the grain size used for removing the elastic peak. Including the grain size in the fitting procedure—as proposed in Ref. 51—failed, because no global optimum could be found. However, it was found that the energy transfer parameters of the biexponential fit were very stable as long as the energy grain of the histogram was not extremely fine (too much elastic collisions included) or extremely coarse (too many collisions contributing to the weak collision component are left out because the elastic peak is “too broad”). The region of stability was therefore used as the criterion for the choice of the grain size. An energy grain of about  $(0.4\text{--}0.5) \cdot \langle \Delta E^2 \rangle^{1/2}$  was adequate for this purpose. An example for such a biexponential fit is included in Fig. 7. The parameters for the downward half of the energy transfer probability for a fixed vibrational energy can be found in Table V [the ones for the upward half are directly obtained by Eq. (23)]. It must be emphasized that the parameters for the strong collision term, because of the low number of trajectories transferring large amounts of energy, are not too well defined.

When comparing the parameters of the transition probabilities it can be seen that  $\gamma$  is about three to eight (average value of about four) times higher than  $\alpha$ , which is in agreement with other trajectory results for the  $\text{CS}_2 + \text{CO}$  and the  $\text{HO}_2 + \text{helium}$  systems.<sup>62,65</sup> The fraction  $x$  of the strong collision component decreases from helium to xenon; in fact, for xenon as bath gas, a monoexponential fit can give a comparably good description of  $P(E, E')$ . The character of  $P(E, E')$  can also explain the trends for  $\langle \Delta E^2 \rangle^{1/2}$  found in Figs. 4 and 5. The result for benzene+argon is a good example: Although the  $\langle \Delta E \rangle$  from the trajectories is nearly equal to the value from experiment,  $\langle \Delta E^2 \rangle^{1/2}$  is higher than the corresponding “experimental” value, which was calculated via a transformation of the experimental  $\langle \Delta E \rangle$  using a monoexponential  $P(E, E')$ . For biexponential transition probabilities this is an expected, characteristic result.

The trajectory values for the fraction of supercollisions are surprisingly high when compared to the results of KCSI

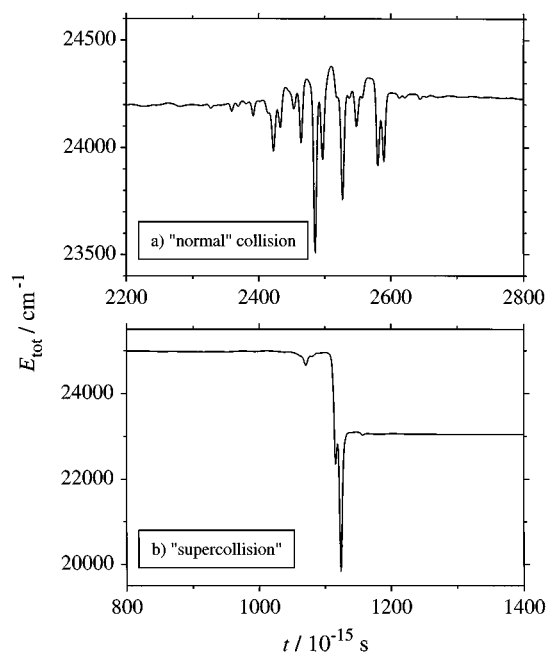


FIG. 8. Time evolution of the benzene energy during two collision events with the bath gas argon, vibrational energy  $E' = 24\,000\text{ cm}^{-1}$ ; (a) “normal” collision showing the typical quasirandom changes of the substrate energy as the argon interacts with the benzene molecule, the energy jumps arise from the interaction of the bath gas atom as it closely approaches one or more substrate atoms, which have random vibrational phases; (b) supercollision from the tail of the transition probability, the final close interaction is significant in determining the amount of energy transferred; note that the time axes have different numbers; each axis showing a time interval of 600 fs.

experiments for toluene colliding with noble gases.<sup>50</sup> These experiments—so far the only ones providing full experimental  $P(E, E')$  distributions—show that the fraction of supercollisions is lower than 1%. Thus the question remains: what leads to this discrepancy? To really answer it, more extended trajectory calculations are necessary to provide larger numbers of low probability energy transfer events and to study the role of the particular influence of the intermolecular potential with respect to supercollisions. However, in any case the surprisingly high fraction  $x$  in the supercollision part of the biexponential fitting expression [Eq. (21)] is *not* simply due to arbitrariness related with the omission of the elastic peak, as has been already discussed further above.

## 2. Mechanistic aspects of supercollisions observed in trajectory calculations

A trajectory calculation can be used both for direct comparison with experiment and to gain dynamical information that can be used for mechanistic understanding. Here, we use our data to obtain a qualitative understanding of the phenomenon of supercollisions.

Data useful for comparing “normal” collisions and supercollisions in the benzene/argon system are shown in Fig. 8, as the time evolution of the energy of the substrate molecule during the collision events. Figure 8(a) shows the pseudorandom variation of total energy with time that is the basis of the biased random walk model.<sup>66–68</sup> The energy jumps

arise from the interaction of the bath gas atom as it closely approaches one or more substrate atoms which have random vibrational phases. These large jumps occur over a comparatively short time, when the argon and one hydrogen approach very closely. This time is approximately that of a C–H stretching period (about  $10^{-14}$  s). For supercollisions in the tail of the transition probability it is found that it is the final close interaction that is significant in determining the amount of energy transferred [Fig. 8(b)].

Earlier work<sup>66–69</sup> has shown that trajectories of the type of Fig. 8(a) are characterized by an autocorrelation function of  $E_{\text{tot}}(t)$  having an approximately exponential form: The total energy in an “average” collision changes essentially in a random fashion while there is significant interaction between the colliding moieties. In contrast to this, the different behavior of Fig. 8(b), when the random peregrinations terminate abruptly, gives an autocorrelation function which is non-exponential. Indeed, the limit of a supercollision which transfers a very large amount of energy would be characterized by an autocorrelation function which is a delta function. The autocorrelation analysis of the trajectory, therefore, may be useful in distinguishing normal from supercollisions. Alternatively, the comparison of  $\langle \Delta E \rangle$  and  $\langle \Delta E^2 \rangle^{1/2}$  may provide useful criteria for this distinction.

## V. CONCLUSIONS

Quasiclassical trajectory calculations have been used to study the deactivation of highly vibrationally excited benzene and HFB molecules in collisions with the noble gases helium, argon, and xenon. It is found that deactivation of benzene is significantly less easy than HFB, a trend which is observed for all bath gases. This result is in agreement with data from direct energy transfer experiments.<sup>10,18–20</sup> Systematic variation of single properties (masses, molecular geometry, the intramolecular, and the intermolecular potential) of the benzene+argon and HFB+argon systems demonstrated that the increase in  $-\langle \Delta E \rangle$  and  $\langle \Delta E^2 \rangle^{1/2}$  for HFB is caused mainly by the mass change on substitution of the hydrogen atoms by fluorine atoms. The perfluorination leads to an extreme drop of the vibrational frequencies, which is much greater than for deuteration. This suggests that the efficiency of collisional energy transfer is enhanced by the presence of low lying vibrational frequencies. The direct correlation between the distribution of the vibrational frequencies and the energy transfer parameters can be extended to other benzene analogous molecules like toluene- $h_8$  and toluene- $d_8$ .

Rotational energy transfer is found to be of similar size for both molecules. A detailed study of the energy transfer for a wide range of initial vibrational and rotational energies and a thermal translational Boltzmann distribution shows that gain and loss of vibrational and rotational energy of the vibrationally hot substrate molecules can be qualitatively related to temperature differences between the translational, rotational and vibrational degrees of freedom. In the systems studied the translational temperature is always low ( $T_{\text{trans}}=300$  K). For high vibrational and low rotational temperatures the vibrations lose energy by vibrational energy transfer ( $\langle \Delta E_{\text{vib}} \rangle < 0$ ); at the same time rotations may heat up to some extent ( $\langle \Delta E_{\text{rot}} \rangle > 0$ ). At very high vibrational and

rotational temperatures both the vibrations and rotations lose energy ( $\langle \Delta E_{\text{vib}} \rangle < 0$ ,  $\langle \Delta E_{\text{rot}} \rangle < 0$ ). For substrate–bath gas systems with sufficient coupling (argon and xenon as a collider) rotational energy transfer leads to a clearly suprathermal steady state rotational temperature after only a few collisions.  $\langle \Delta E_{\text{vib}} \rangle$  is nearly independent of rotational energy for rotational temperatures up to approximately 450 K and for rotational distributions of different shape (e.g., canonical and microcanonical). With regard to our type of trajectory calculations, which refer to an ensemble of isolated collisions,  $\langle \Delta E_{\text{vib}} \rangle$  turns out to be the correct quantity for comparison with IRF and UVA experiments, in which—because of the presence of a cascade of collisions—the rotational steady state will be rapidly established.

$\langle \Delta E \rangle$  and  $\langle \Delta E^2 \rangle^{1/2}$  increase with increasing vibrational energy for HFB and benzene. Qualitative but not completely quantitative agreement between calculation and experiment is reached for the absolute  $\langle \Delta E \rangle$  and  $\langle \Delta E^2 \rangle^{1/2}$  values using a LJ 12-6 potential. However, the measured and calculated bath gas dependences are different. From helium to xenon the experimental  $-\langle \Delta E \rangle$  and  $\langle \Delta E^2 \rangle^{1/2}$  are increasing whereas for the calculated values the opposite trend is observed. This result is independent of the excited molecule. Two different intermolecular potentials of a EXP-6 type have been tested with the parameters of the repulsive exponential interaction taken from *ab initio* quantum mechanical calculations.<sup>44</sup> It has been shown that the main determinant of the amount of energy transferred, for a given type of potential, is the steepness of the repulsive part; for a given potential, the masses of the atoms in the system exert a strong influence on the energy transfer, by changing the values of the lowest vibrational frequencies. The energy transfer probabilities can be described by biexponential fits. The calculated fractions of strong collisions appear to be markedly higher than found in the newest experimental results for toluene colliding with noble gases.<sup>50</sup>

## ACKNOWLEDGMENTS

Helpful comments by David L. Clarke, Gregory T. Russell, Horst Hippler, and Jörg Schroeder are much appreciated. Financial support by the Deutsche Forschungsgemeinschaft (Sonderforschungsbereich 357: “Molekulare Mechanismen Unimolekularer Prozesse”) and the Australian Research Council is gratefully acknowledged.

## APPENDIX A: INTRAMOLECULAR POTENTIAL PARAMETERS AND VIBRATIONAL FREQUENCIES

The equilibrium bond lengths  $r_e$ , equilibrium bond angles  $\Theta_e$ , stretching force constants  $f_s$ , bending force constants  $f_\Theta$ , wagging force constants  $f_\alpha$ , and torsional barriers  $V_0$  for benzene and HFB are tabulated in the following:<sup>36–39</sup>  
Benzene:

$$\text{CH-stretch: } r_e = 1.084 \text{ \AA}, \quad f_s = 5.076 \text{ mdyn \AA}^{-1};$$

$$\text{CC-stretch: } r_e = 1.397 \text{ \AA}, \quad f_s = 6.640 \text{ mdyn \AA}^{-1};$$

$$\text{CCH-bend: } \Theta_e = 120^\circ, \quad f_\Theta = 0.521 \text{ mdyn \AA rad}^{-2};$$

$$\text{CCC-bend: } \Theta_e = 120^\circ, \quad f_\Theta = 1.065 \text{ mdyn \AA rad}^{-2};$$

$$\text{CCH-wag: } f_\alpha = 0.297 \text{ mdyn } \text{\AA} \text{ rad}^{-2};$$

$$\text{torsion: } V_0 = 24.0 \text{ kcal mol}^{-1}.$$

HFB:

$$\text{CF-stretch: } r_e = 1.327 \text{ \AA}, \quad f_s = 6.640 \text{ mdyn } \text{\AA}^{-1};$$

$$\text{CC-stretch: } r_e = 1.394 \text{ \AA}, \quad f_s = 5.800 \text{ mdyn } \text{\AA}^{-1};$$

$$\text{CCF-bend: } \Theta_e = 120^\circ, \quad f_\Theta = 0.800 \text{ mdyn } \text{\AA} \text{ rad}^{-2};$$

$$\text{CCC-bend: } \Theta_e = 120^\circ, \quad f_\Theta = 1.550 \text{ mdyn } \text{\AA} \text{ rad}^{-2};$$

$$\text{CCF-wag: } f_\alpha = 0.297 \text{ mdyn } \text{\AA} \text{ rad}^{-2};$$

$$\text{torsion: } V_0 = 24.0 \text{ kcal mol}^{-1}.$$

Using these parameters one obtains the following VFF vibrational frequencies  $\nu$  (in  $\text{cm}^{-1}$ ), assignments and zero point energies  $E_z$  (in  $\text{cm}^{-1}$ ) of benzene and HFB. Experimental values are given in parentheses.<sup>36,39</sup> The normal modes of  $E$  symmetry are doubly degenerated:

Benzene:

$$\nu_1(A_{1g}) = 3057(3073), \quad \nu_{2,3}(E_{1u}) = 3057(3068),$$

$$\nu_{4,5}(E_{2g}) = 3059(3056),$$

$$\nu_6(B_{1u}) = 3060(3057), \quad \nu_{7,8}(E_{2g}) = 1739(1600),$$

$$\nu_{9,10}(E_{1u}) = 1531(1482),$$

$$\nu_{11}(A_{2g}) = 1376(1350), \quad \nu_{12}(B_{2u}) = 1749(1309),$$

$$\nu_{13,14}(E_{2g}) = 1134(1178),$$

$$\nu_{15}(B_{2u}) = 1173(1146), \quad \nu_{16,17}(E_{1u}) = 991(1037),$$

$$\nu_{18}(B_{1u}) = 1026(1010),$$

$$\nu_{19}(A_{1g}) = 926(993), \quad \nu_{20,21}(E_{2g}) = 617(606),$$

$$\nu_{22}(B_{2g}) = 1070(990),$$

$$\nu_{23,24}(E_{2u}) = 1015(967), \quad \nu_{25,26}(E_{1g}) = 833(846),$$

$$\nu_{27}(B_{2g}) = 657(707),$$

$$\nu_{28}(A_{2u}) = 680(673), \quad \nu_{29,30}(E_{2u}) = 400(398),$$

$$E_Z = 21\,763(21\,392).$$

HFB:

$$\nu_1(A_{1g}) = 1457(1490), \quad \nu_{2,3}(E_{1u}) = 1598(1530),$$

$$\nu_{4,5}(E_{2g}) = 1183(1157),$$

$$\nu_6(B_{1u}) = 1698(1323), \quad \nu_{7,8}(E_{2g}) = 1821(1655),$$

$$\nu_{9,10}(E_{1u}) = 929(1007),$$

$$\nu_{11}(A_{2g}) = 755(691), \quad \nu_{12}(B_{2u}) = 1610(1253),$$

$$\nu_{13,14}(E_{2g}) = 271(264),$$

$$\nu_{15}(B_{2u}) = 278(208), \quad \nu_{16,17}(E_{1u}) = 285(315),$$

$$\nu_{18}(B_{1u}) = 592(640),$$

$$\nu_{19}(A_{1g}) = 479(559), \quad \nu_{20,21}(E_{2g}) = 444(443),$$

$$\nu_{22}(B_{2g}) = 772(714),$$

$$\nu_{23,24}(E_{2u}) = 608(595), \quad \nu_{25,26}(E_{1g}) = 379(370),$$

$$\nu_{27}(B_{2g}) = 172(249),$$

$$\nu_{28}(A_{2u}) = 197(210), \quad \nu_{29,30}(E_{2u}) = 126(120),$$

$$E_Z = 11\,649(11\,124).$$

## APPENDIX B: INTERMOLECULAR POTENTIAL PARAMETERS

The Lennard-Jones and EXP-6 potential parameters for benzene and HFB interacting with the monoatomic bath gases helium, argon and xenon can be found in the following. The values for  $C$  and  $\eta$  are from quantum chemical calculations.<sup>44</sup> Also the resulting potential-dependent effective collision diameters  $\sigma_{\text{eff}}$  and well depths  $\epsilon_{\text{eff}}$  for the different molecule–bath gas systems are given, both obtained from the model potentials by numerical integration using midordinate rule on a six-point grid.<sup>29,45</sup> The reference collision numbers  $Z_{\text{ref}}$  are the ones used in the benzene and HFB experiments<sup>10,20</sup>

$$\text{Helium: } \sigma_M = 2.55 \text{ \AA}, \quad \epsilon_M/k_B = 10.22 \text{ K. Neon: } \sigma_M = 2.82 \text{ \AA}, \quad \epsilon_M/k_B = 32.0 \text{ K.}$$

$$\text{Argon: } \sigma_M = 3.47 \text{ \AA}, \quad \epsilon_M/k_B = 113.5 \text{ K. Xenon: } \sigma_M = 4.05 \text{ \AA}, \quad \epsilon_M/k_B = 230.0 \text{ K.}$$

Benzene+helium:

$$\sigma_{C-\text{He}} = 2.9170 \text{ \AA}, \quad \sigma_{\text{H-He}} = 2.7703 \text{ \AA}, \quad \epsilon_{C-\text{He}}/k_B = 15.7185 \text{ K}, \quad \epsilon_{\text{H-He}}/k_B = 8.8831 \text{ K}, \quad \lambda_1 = 1.0864, \quad \lambda_2 = 0.8692,$$

$$C_{C-\text{He}}/k_B = 33.5477 \times 10^6 \text{ K}, \quad C_{\text{H-He}}/k_B = 5.2690 \times 10^6 \text{ K}, \quad \eta_{C-\text{He}} = 3.4010 \text{ \AA}^{-1}, \quad \eta_{\text{H-He}} = 3.3003 \text{ \AA}^{-1}, \quad A = 2.7603,$$

$$\text{LJ12-6: } \sigma_{\text{eff}} = 4.01 \text{ \AA}, \quad \epsilon_{\text{eff}}/k_B = 64 \text{ K}, \quad \text{AHL-1: } \sigma_{\text{eff}} = 5.11 \text{ \AA}, \quad \epsilon_{\text{eff}}/k_B = 12 \text{ K};$$

$$\text{AHL-2: } \sigma_{\text{eff}} = 4.51 \text{ \AA}, \quad \epsilon_{\text{eff}}/k_B = 64 \text{ K}, \quad Z_{\text{ref}} = 6.099 \times 10^{-10} \text{ cm}^3 \text{ s}^{-1}.$$

Benzene+argon:

$$\sigma_{C-\text{Ar}} = 3.3872 \text{ \AA}, \quad \sigma_{\text{H-Ar}} = 3.2418 \text{ \AA}, \quad \epsilon_{C-\text{Ar}}/k_B = 48.1695 \text{ K}, \quad \epsilon_{\text{H-Ar}}/k_B = 27.2221 \text{ K}, \quad \lambda_1 = 1.0770, \lambda_2 = 0.7793,$$

$$C_{C-\text{Ar}}/k_B = 36.0745 \times 10^6 \text{ K}, \quad C_{\text{H-Ar}}/k_B = 7.0734 \times 10^6 \text{ K}, \quad \eta_{C-\text{Ar}} = 3.1208 \text{ \AA}^{-1}, \quad \eta_{\text{H-Ar}} = 3.0217 \text{ \AA}^{-1}, \quad A = 2.0564,$$

$$\text{LJ12-6: } \sigma_{\text{eff}} = 4.47 \text{ \AA}, \quad \epsilon_{\text{eff}}/k_B = 213 \text{ K}; \quad \text{AHL-1: } \sigma_{\text{eff}} = 5.36 \text{ \AA}, \quad \epsilon_{\text{eff}}/k_B = 63 \text{ K};$$



AHL-2:  $\sigma_{\text{eff}}=4.89 \text{ \AA}$ ,  $\epsilon_{\text{eff}}/k_{\text{B}}=213 \text{ K}$ ,  $Z_{\text{ref}}=4.148 \cdot 10^{-10} \text{ cm}^3 \text{ s}^{-1}$ .

Benzene+xenon:

$\sigma_{\text{C-Xe}}=3.6874 \text{ \AA}$ ,  $\sigma_{\text{H-Xe}}=3.5425 \text{ \AA}$ ,  $\epsilon_{\text{C-Xe}}/k_{\text{B}}=65.3354 \text{ K}$ ,  $\epsilon_{\text{H-Xe}}/k_{\text{B}}=36.9232 \text{ K}$ ,  $\lambda_1=1.0735$ ,  $\lambda_2=0.7616$ ,

LJ12-6:  $\sigma_{\text{eff}}=4.78 \text{ \AA}$ ,  $\epsilon_{\text{eff}}/k_{\text{B}}=304 \text{ K}$ ,  $Z_{\text{ref}}=4.100 \times 10^{-10} \text{ cm}^3 \text{ s}^{-1}$ .

HFB+helium:

$\sigma_{\text{C-He}}=3.0093 \text{ \AA}$ ,  $\sigma_{\text{F-He}}=3.0093 \text{ \AA}$ ,  $\epsilon_{\text{C-He}}/k_{\text{B}}=11.9494 \text{ K}$ ,  $\epsilon_{\text{F-He}}/k_{\text{B}}=11.9494 \text{ K}$ ,  $\lambda_1=1.1208$ ,  $\lambda_2=0.6608$ ,

$C_{\text{C-He}}/k_{\text{B}}=33.5477 \times 10^6 \text{ K}$ ,  $C_{\text{F-He}}/k_{\text{B}}=49.1746 \times 10^6 \text{ K}$ ,  $\eta_{\text{C-He}}=3.4010 \text{ \AA}^{-1}$ ,  $\eta_{\text{F-He}}=4.3063 \text{ \AA}^{-1}$ ,  $A=1.4677$ ,

LJ12-6:  $\sigma_{\text{eff}}=4.37 \text{ \AA}$ ,  $\epsilon_{\text{eff}}/k_{\text{B}}=57 \text{ K}$ ; AHL-1:  $\sigma_{\text{eff}}=4.77 \text{ \AA}$ ,  $\epsilon_{\text{eff}}/k_{\text{B}}=30 \text{ K}$ ;

AHL-2:  $\sigma_{\text{eff}}=4.57 \text{ \AA}$ ,  $\epsilon_{\text{eff}}/k_{\text{B}}=57 \text{ K}$ .  $Z_{\text{ref}}=7.009 \times 10^{-10} \text{ cm}^3 \text{ s}^{-1}$ .

HFB+argon:

$\sigma_{\text{C-Ar}}=3.4752 \text{ \AA}$ ,  $\sigma_{\text{F-Ar}}=3.4752 \text{ \AA}$ ,  $\epsilon_{\text{C-Ar}}/k_{\text{B}}=36.3507 \text{ K}$ ,  $\epsilon_{\text{F-Ar}}/k_{\text{B}}=36.3507 \text{ K}$ ,  $\lambda_1=1.1050$ ,  $\lambda_2=0.6032$ ,

$C_{\text{C-Ar}}/k_{\text{B}}=36.0745 \times 10^6 \text{ K}$ ,  $C_{\text{F-Ar}}/k_{\text{B}}=68.1565 \times 10^6 \text{ K}$ ,  $\eta_{\text{C-Ar}}=3.1208 \text{ \AA}^{-1}$ ,  $\eta_{\text{F-Ar}}=3.8667 \text{ \AA}^{-1}$ ,  $A=1.2715$ ,

LJ12-6:  $\sigma_{\text{eff}}=4.83 \text{ \AA}$ ,  $\epsilon_{\text{eff}}/k_{\text{B}}=191 \text{ K}$ ; AHL-1:  $\sigma_{\text{eff}}=5.09 \text{ \AA}$ ,  $\epsilon_{\text{eff}}/k_{\text{B}}=128 \text{ K}$ ;

AHL-2:  $\sigma_{\text{eff}}=4.96 \text{ \AA}$ ,  $\epsilon_{\text{eff}}/k_{\text{B}}=191 \text{ K}$ .  $Z_{\text{ref}}=4.155 \times 10^{-10} \text{ cm}^3 \text{ s}^{-1}$ .

HFB+xenon:

$\sigma_{\text{C-Xe}}=3.7734 \text{ \AA}$ ,  $\sigma_{\text{H-Xe}}=3.7734 \text{ \AA}$ ,  $\epsilon_{\text{C-Xe}}/k_{\text{B}}=49.1980 \text{ K}$ ,  $\epsilon_{\text{H-Xe}}/k_{\text{B}}=49.1980 \text{ K}$ ,  $\lambda_1=1.0985$ ,  $\lambda_2=0.5735$ ,

LJ12-6:  $\sigma_{\text{eff}}=5.12 \text{ \AA}$ ,  $\epsilon_{\text{eff}}/k_{\text{B}}=273 \text{ K}$ .  $Z_{\text{ref}}=3.588 \times 10^{-10} \text{ cm}^3 \text{ s}^{-1}$ .

<sup>1</sup>B. S. Rabinovitch and D. C. Tardy, *Chem. Rev.* **77**, 369 (1977).

<sup>2</sup>M. Quack and J. Troe, in *Gas Kinetics and Energy Transfer*, edited by P. G. Ashmore and R. J. Donovan (The Chemical Society, London 1977), Vol. 2.

<sup>3</sup>I. Oref and D. C. Tardy, *Chem. Rev.* **90**, 1407 (1990).

<sup>4</sup>H. Hippler and J. Troe, in *Bimolecular Collisions*, edited by J. E. Baggott and M. N. R. Ashfold (The Royal Society of Chemistry, London, 1989).

<sup>5</sup>H. Hippler, J. Troe, and H. J. Wendelken, *J. Chem. Phys.* **78**, 6709 (1983).

<sup>6</sup>K. Luther and K. Reihs, *Ber. Bunsenges. Phys. Chem.* **92**, 442 (1988).

<sup>7</sup>B. M. Toselli and J. R. Barker, *Chem. Phys. Lett.* **174**, 304 (1990).

<sup>8</sup>B. M. Toselli, J. D. Brenner, M. L. Yerram, W. E. Chin, K. D. King, and J. R. Barker, *J. Chem. Phys.* **95**, 176 (1991).

<sup>9</sup>B. M. Toselli and J. R. Barker, *J. Chem. Phys.* **95**, 8108 (1991).

<sup>10</sup>B. M. Toselli and J. R. Barker, *J. Chem. Phys.* **97**, 1809 (1992).

<sup>11</sup>M. Damm, F. Deckert, H. Hippler, and J. Troe, *J. Phys. Chem.* **95**, 2005 (1991).

<sup>12</sup>H. Hippler, B. Otto, and J. Troe, *Ber. Bunsenges. Phys. Chem.* **93**, 428 (1989).

<sup>13</sup>H. Hippler, L. Lindemann, and J. Troe, *J. Chem. Phys.* **83**, 3906 (1985).

<sup>14</sup>M. J. Rossi, J. P. Pladziewicz, and J. R. Barker, *J. Chem. Phys.* **78**, 6695 (1983).

<sup>15</sup>J. R. Barker, *J. Phys. Chem.* **88**, 11 (1984).

<sup>16</sup>J. R. Barker and R. E. Golden, *J. Phys. Chem.* **88**, 1012 (1984).

<sup>17</sup>J. Shi and J. R. Barker, *J. Chem. Phys.* **88**, 6219 (1988).

<sup>18</sup>M. L. Yerram, J. D. Brenner, K. D. King, and J. R. Barker, *J. Phys. Chem.* **94**, 6341 (1990).

<sup>19</sup>J. D. Brenner, J. P. Erinjeri, and J. R. Barker, *Chem. Phys.* **175**, 99 (1993).

<sup>20</sup>M. Damm, H. Hippler, H. A. Olschewski, J. Troe, and J. Willner, *Z. Phys. Chem. N. F.* **166**, 129 (1990).

<sup>21</sup>N. Nakashima and K. Yoshihara, *J. Chem. Phys.* **79**, 2727 (1983).

<sup>22</sup>T. Ichimura, M. Takahashi, and Y. Mori, *Chem. Phys. Lett.* **114**, 111 (1987).

<sup>23</sup>T. Ichimura, Y. Mori, N. Nakashima, and K. Yoshihara, *J. Chem. Phys.* **83**, 117 (1985).

<sup>24</sup>T. Ichimura, Y. Mori, N. Nakashima, and K. Yoshihara, *Chem. Phys. Lett.* **104**, 533 (1984).

<sup>25</sup>D. L. Clarke, I. Oref, R. G. Gilbert, and K. F. Lim, *J. Chem. Phys.* **96**, 5983 (1992).

<sup>26</sup>D. L. Clarke and R. G. Gilbert, *J. Phys. Chem.* **96**, 8450 (1992).

<sup>27</sup>K. F. Lim and R. G. Gilbert, *J. Phys. Chem.* **94**, 72 (1990).

<sup>28</sup>K. F. Lim and R. G. Gilbert, *J. Phys. Chem.* **94**, 77 (1990).

<sup>29</sup>K. F. Lim, *J. Chem. Phys.* **100**, 7385 (1994).

<sup>30</sup>K. F. Lim, *J. Chem. Phys.* **101**, 8756 (1994).

<sup>31</sup>R. G. Gilbert, *Aust. J. Chem.* (to be published).

<sup>32</sup>J. M. Morgulis, S. S. Sapers, C. Steel, and I. Oref, *J. Chem. Phys.* **90**, 923 (1989).

<sup>33</sup>G. H. Kohlmaier and B. S. Rabinovitch, *J. Chem. Phys.* **38**, 1692 (1963).

<sup>34</sup>M. Bruehl and G. C. Schatz, *J. Chem. Phys.* **89**, 770 (1988).

<sup>35</sup>M. Bruehl and G. C. Schatz, *J. Phys. Chem.* **92**, 7223 (1988).

<sup>36</sup>V. J. Eaton and D. Steele, *J. Mol. Spectrosc.* **48**, 446 (1973).

<sup>37</sup>A. Almenningen, O. Bastiansen, R. Seip, and H. M. Seip, *Acta Chem. Scand.* **18**, 2115 (1964).

<sup>38</sup>J. A. Draeger, *Spectrochim. Acta Part A* **41**, 607 (1985).

<sup>39</sup>R. A. R. Pearce, D. Steele, and K. Radcliffe, *J. Mol. Struct.* **15**, 409 (1973).

<sup>40</sup>M. Henkel, B. Pfeil, and W. Seidel, *J. Chem. Phys.* **96**, 5054 (1992).

<sup>41</sup>L. J. Danielson, M. Keil, and P. J. Dunlop, *J. Chem. Phys.* **88**, 4218 (1988).

<sup>42</sup>R. Brandt, M. Henkel, B. Pfeil, and W. Seidel, *J. Chem. Phys.* **95**, 135 (1991).

<sup>43</sup>H. J. Böhm, R. Ahlrichs, P. Scharf, and H. Schiffer, *J. Chem. Phys.* **81**, 1389 (1984).

<sup>44</sup>H. J. Böhm and R. Ahlrichs, *J. Chem. Phys.* **77**, 2028 (1982).

<sup>45</sup>K. F. Lim, *Program SIGMON: An Aid for the Semiempirical Fitting of the Intermolecular Potential*. Available from K. F. Lim, School of Chemistry, University of Melbourne, Parkville, VIC 3052, Australia (1992).

<sup>46</sup>W. L. Hase, R. J. Duchovic, X. Hu, K. F. Lim, D.-H. Lu, G. H. Peslherbe, K. N. Swamy, S. R. Vande Linde, H. Wang, and R. J. Wolf, *Program VENUS: A General Chemical Dynamics Computer Program*, Quantum Chem. Program Exchange Bull. (to be submitted).

<sup>47</sup>W. Forst, *J. Chem. Phys.* **80**, 2504 (1984).

<sup>48</sup>W. Forst and J. R. Barker, *J. Chem. Phys.* **83**, 124 (1985).

<sup>49</sup>J. Troe, *J. Chem. Phys.* **77**, 3485 (1982).

<sup>50</sup>T. Lenzer, K. Luther, A. Symonds, and J. Troe, *J. Chem. Phys.* (to be submitted).

<sup>51</sup>H. Hippler, H. W. Schranz, and J. Troe, *J. Phys. Chem.* **90**, 6158 (1986).

- <sup>52</sup>H. W. Schranz and J. Troe, *J. Phys. Chem.* **90**, 6168 (1986).
- <sup>53</sup>B. Efron, *SIAM Rev.* **90**, 460 (1979).
- <sup>54</sup>P. Diaconis and B. Efron, *Sci. Am.* **248**(5), 96 (May, 1983).
- <sup>55</sup>K. F. Lim, *Program PEERAN: P(E,E') Error Analysis Program*, Available from K. F. Lim, School of Chemistry, University of Melbourne, Parkville, VIC 3052, Australia (1993); email kieran\_lim.chemistry@muwayf.unimelb.edu.au.
- <sup>56</sup>L. Landau, E. Teller, *Phys. Z. Sowjetunion* **10**, 34 (1936).
- <sup>57</sup>R. N. Schwartz, Z. I. Slawsky, and K. F. Herzfeld, *J. Chem. Phys.* **20**, 1591 (1952).
- <sup>58</sup>R. N. Schwartz, Z. I. Slawsky, and K. F. Herzfeld, *J. Chem. Phys.* **22**, 767 (1954).
- <sup>59</sup>R. G. Gilbert and R. N. Zare, *Chem. Phys. Lett.* **167**, 407 (1990).
- <sup>60</sup>D. L. Clarke, K. C. Thompson, and R. G. Gilbert, *Chem. Phys. Lett.* **182**, 357 (1991).
- <sup>61</sup>L. Lendvay and G. C. Schatz, *J. Phys. Chem.* **94**, 8864 (1990).
- <sup>62</sup>L. Lendvay and G. C. Schatz, *J. Phys. Chem.* **98**, 6530 (1994).
- <sup>63</sup>J. Troe, *J. Chem. Phys.* **97**, 288 (1992).
- <sup>64</sup>MicroCal Software, *Program ORIGIN*. Available from MicroCal Software, Inc., Northampton, MA 01060 (1993).
- <sup>65</sup>N. J. Brown and J. A. Miller, *J. Chem. Phys.* **80**, 5568 (1984).
- <sup>66</sup>R. G. Gilbert, *J. Chem. Phys.* **80**, 5501 (1984).
- <sup>67</sup>K. F. Lim and R. G. Gilbert, *J. Chem. Phys.* **84**, 6129 (1986).
- <sup>68</sup>K. F. Lim and R. G. Gilbert, *J. Chem. Phys.* **92**, 1819 (1990).
- <sup>69</sup>R. G. Gilbert, *Int. Rev. Phys. Chem.* **10**, 319 (1991).